JOURNAL OF GEOPHYSICAL RESEARCH, VOL. 105, NO. C3, PAGES 6387–6414, MARCH 15, 2000

Character and dynamics of the Red Sea and Persian Gulf outflows

Amy S. Bower, Heather D. Hunt, and James F. Price

Department of Physical Oceanography, Woods Hole Oceanographic Institution, Woods Hole, Massachusetts

Abstract. Historical hydrographic data and a numerical plume model are used to investigate the initial transformation, dynamics, and spreading pathways of Red Sea and Persian Gulf outflow waters where they enter the Indian Ocean. The annual mean transport of these outflows is relatively small (< 0.4 Sv), but they have a major impact on the hydrographic properties of the Indian Ocean at the thermocline level because of their high salinity. They are different from other outflows in that they flow over very shallow sills (depth < 200 m) into a highly stratified upper ocean environment and they are located at relatively low latitudes (12°N and 26°N). Furthermore, the Red Sea outflow exhibits strong seasonal variability in transport. The four main results of this study are as follows. First, on the basis of observed temperature-salinity (T-S) characteristics of the outflow source and product waters we estimate that the Red Sea and Persian Gulf outflows are diluted by factors of ~2.5 and 4, respectively, as they descend from sill depth to their depth of neutral buoyancy. The high-dilution factor for the Persian Gulf outflow results from the combined effects of large initial density difference between the outflow source water and oceanic water and low outflow transport. Second, the combination of low latitude and low outflow transport (and associated low outflow thickness) results in Ekman numbers for both outflows that are O(1). This indicates that they should be thought of as frictional density currents modified by rotation rather than geostrophic density currents modified by friction. Third, different mixing histories along the two channels that direct Red Sea outflow water into the open ocean result in product waters with significantly different densities, which probably contributes to the multilayered structure of the Red Sea product waters. In both outflows, seasonal variations in source water and oceanic properties have some effect on the T-S of the product waters, but they have only a minor impact on equilibrium depth. Fourth, product waters from both outflows are advected away from the sill region in narrow boundary currents, at least during part of the year. At other times, the product water appears more in isolated patches.

1. Introduction

The Red Sea and Persian Gulf are the source regions for two of the most saline water masses found in the world ocean [*Rochford*, 1964]. The salinity of Red Sea Water (RSW) and Persian Gulf Water (PGW) is 40-41 over most of the Red Sea and Persian Gulf and can exceed 50 in limited areas of the latter [see, e.g., *Wyrtki*, 1971; *John et al.*, 1990]. These high salinities are the result of extremely high evaporation (~2 m yr^{-1} [*Privett*, 1959], insignificant rainfall and river inflow, and restricted exchange with the open ocean.

The dense, saline RSW and PGW enter the Indian Ocean in exchange flows through narrow, shallow straits: the former through the Bab-al-Mandeb (BAM) Strait and the latter through the Strait of Hormuz (Figures 1 and 2). They exit the straits as dense bottom currents, cascading down the continental slope and entraining less dense water until they reach neutral buoyancy and spread laterally into the Indian Ocean [see, e.g., *Morcos*, 1970; *Siedler*, 1968; *Chao et al.*, 1992]. Estimates of the annual mean volume transport of RSW and PGW through their respective straits, ~0.4 Sv and ~0.2 Sv [see, e.g., *Siedler*, 1969; *Ahmad and Sultan*, 1991], are small compared to some other marginal sea outflows (e.g., ~1 Sv for the Mediterranean and ~2.5 Sv for the Denmark Strait outflows). Nevertheless, RSW and PGW can be traced at intermediate depths over large portions of the Indian Ocean owing to their extreme temperature-salinity characteristics [*Rochford*, 1964; *Wyrtki*, 1971; *Varma et al.*, 1980; *Premchand et al.*, 1986; *Shapiro and Meshchanov*, 1991; *Beal et al.*, 1999]. RSW spreads into the open Indian Ocean in the depth range 500-800 m, and PGW is found at 200-350 m [*Wyrtki*, 1971]. RSW and PGW are the only two "native" intermediate water masses in the Indian Ocean. They affect the stratification of the upper water column and inject higher-oxygen water into the strong oxygen minimum characteristic of the Arabian Sea [*Wyrtki*, 1971; *Brewer et al.*, 1978].

In addition to their relatively small transport, these two marginal sea outflows are different from the major Atlantic outflows in several other ways. First, they flow over very shallow sills: Sill depth is ~160 m in BAM Strait and ~80 m in the Strait of Hormuz compared to 300 m and deeper for the Atlantic outflows. Thus they are injected into the highly stratified, upper ocean environment. Second, the outflows enter the open ocean at lower latitudes (12°N for the Red Sea, 26°N for the Persian Gulf), which has important implications for the dynamics of the outflows. Third, the Red Sea in

Paper number 1999JC900297.
0148-0227/00/1999JC900297$09.00

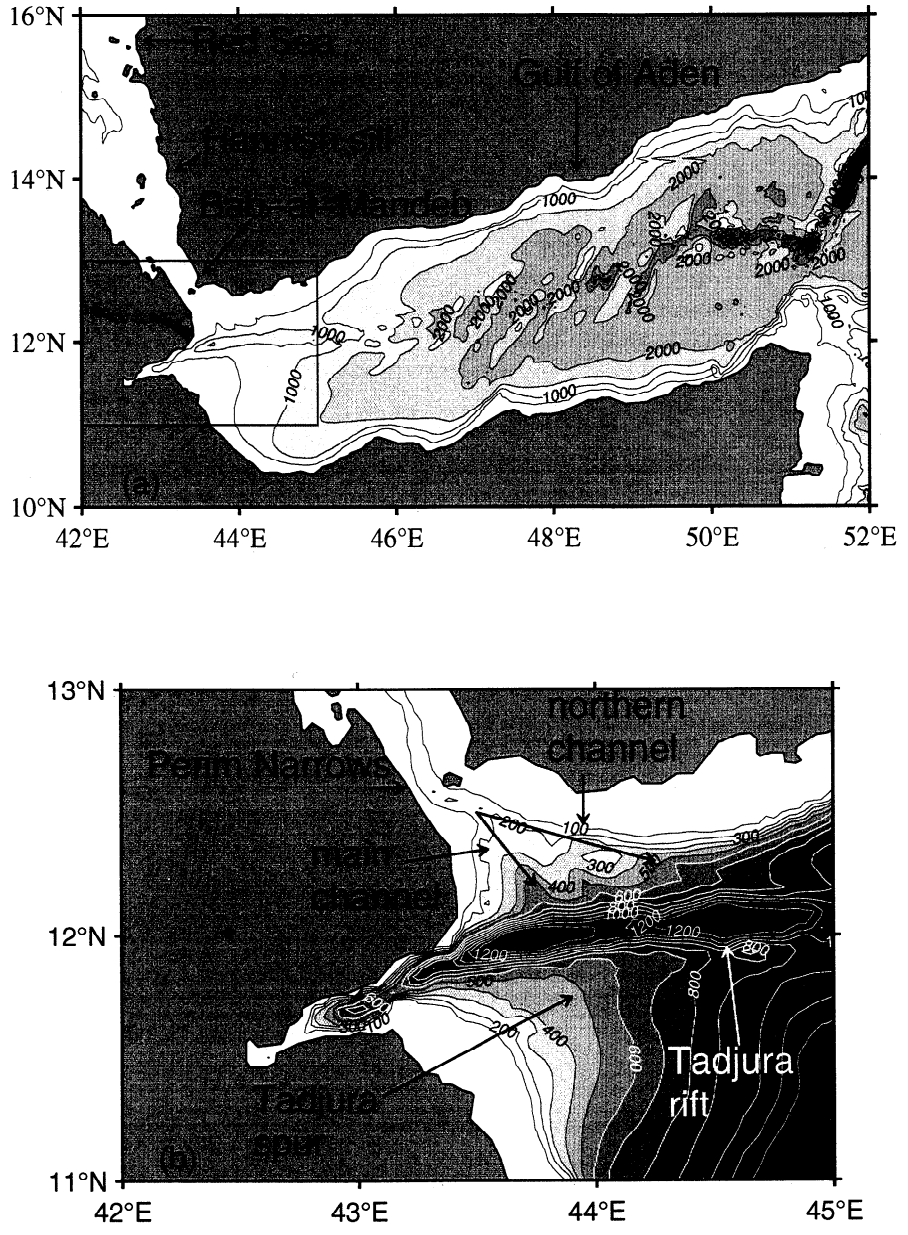

Figure 1. (a) Chart of the southeastern Red Sea, Bab-el-Mandeb (BAM), and the Gulf of Aden. Bathymetry is shaded in 500-m intervals. (b) Expanded view of the southeastern end of BAM Strait and the western Gulf of Aden (area shown by box in Figure 1a). Bathymetry is contoured in 100-m intervals to 1200 m. The two arrows indicate the approximate axes of the two main channels exiting the strait. The northern channel is not well resolved by this ETOPO2 digital bathymetric data set (see text).

particular exhibits significant seasonal variability in transport due to the effects of monsoon winds and seasonal variations in buoyancy fluxes [see, e.g., *Patzert*, 1972a, b; *Osman*, 1985; *Maillard and Soliman*, 1986; *Murray and Johns*, 1997].

Historical observations give only a limited view of the structure of the Red Sea and Persian Gulf outflows in the regions immediately downstream of the straits (i.e., in the Gulf of Aden and Gulf of Oman). *Siedler's* [1968] otherwise comprehensive survey of water properties and currents in BAM Strait did not extend far into the Gulf of Aden. *Fedorov and Meshchanov's* [1988] analysis of historical data from the Gulf of Aden in the former Soviet Union archives is limited in that none of the original data are shown, and their results are illustrated only schematically. There have been no studies of the PGW outflow near the exit of the Strait of Hormuz reported in the literature. From a small number of individual hydrographic sections across the Gulf of Oman, it appears that PGW is often found along the southern boundary of the gulf from 200 m to 400 m [see, e.g., *Premchand et al.*, 1986].

In this study, we use historical hydrographic data from the U. S. Naval Oceanographic Office and the numerical outflow model of *Price and Baringer* [1994] (here-in-after referred to as PB94) to investigate the transformation, dynamics, and initial spreading pathways of the Red Sea and Persian Gulf outflows where they enter the Indian Ocean. Specifically, we have first combined an analysis of historical observations with

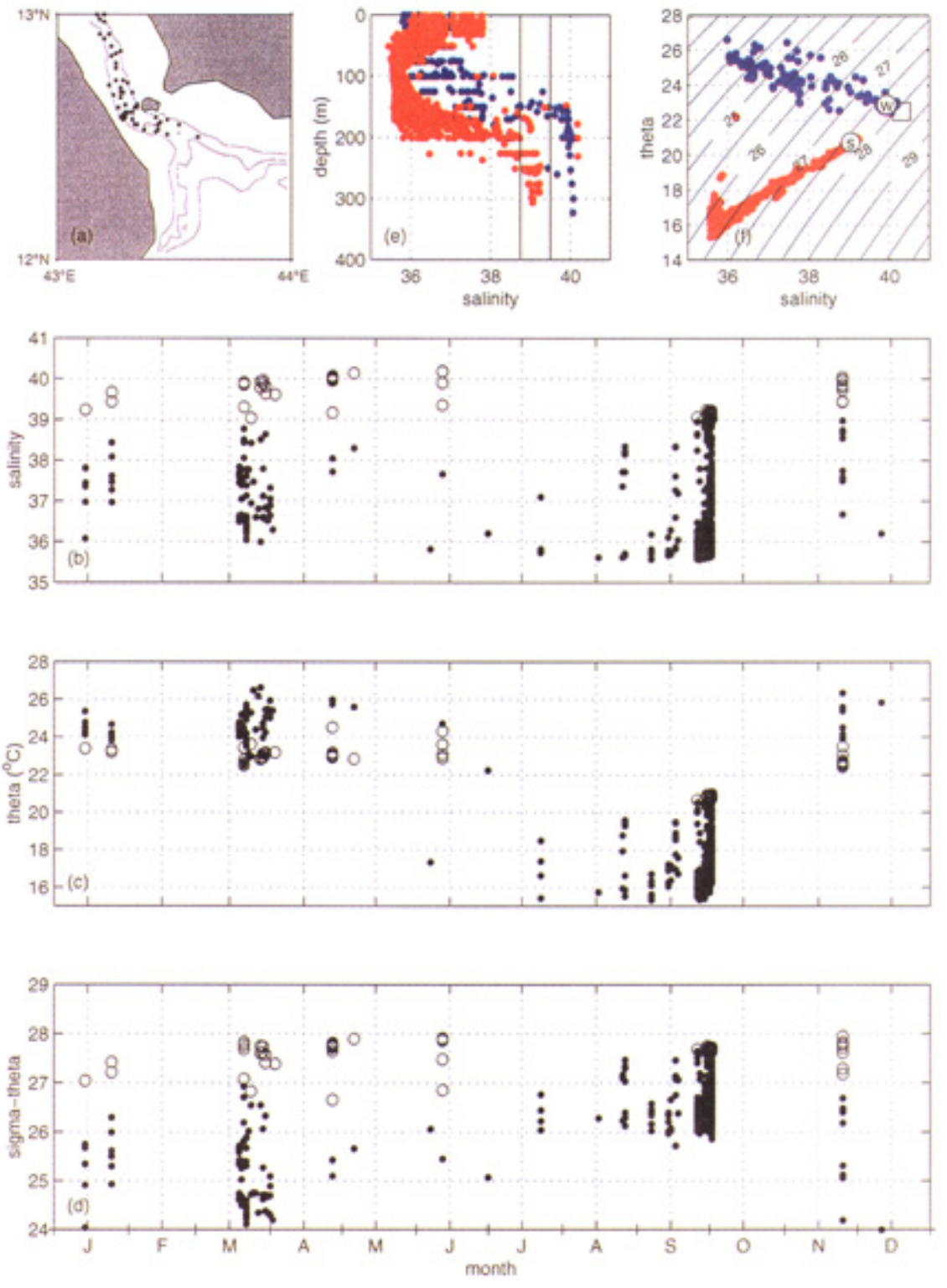

Plate 1. (a) Positions of hydrographic observations deeper than 100 m in the Perim Narrows region. 100 m, 200 m and 300 m isobaths are superimposed. (b-d) Salinity, potential temperature, and potential density below 100 m in the narrows as a function of day of year. The open circles indicate observations with $S > 39$. (e) Salinity versus depth for all observations in the narrows. Blue corresponds to winter observations, and red corresponds to summer. The vertical lines indicate the lower salinity limit for averaging: 38.75 for summer and 39.5 for winter. (f) *T-S* diagram showing winter (blue) and summer (red) observations in the narrows from below 100 m. Circles indicate mean winter and summer values for the Red Sea outflow water, and the square represents the *T-S* properties at the Hanish sill.

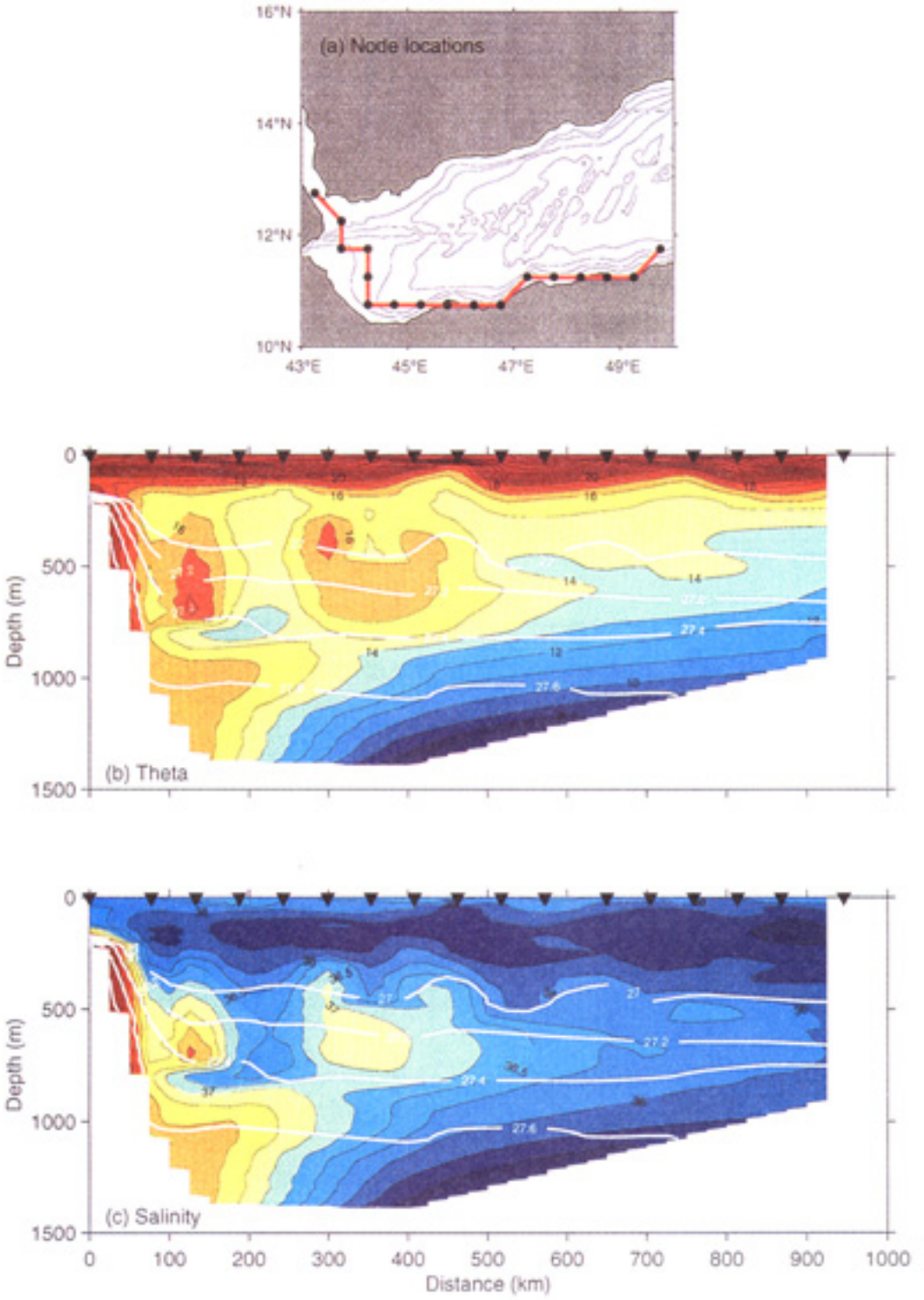

Plate 2. (a) Location of section along path of Red Sea outflow. Bathymetric contours are shown every 500 m. (b) Potential temperature and (c) salinity along the section shown in (Plate 2a) obtained by averaging hydrographic data in 0.5° squares. Four potential density contours are superimposed.

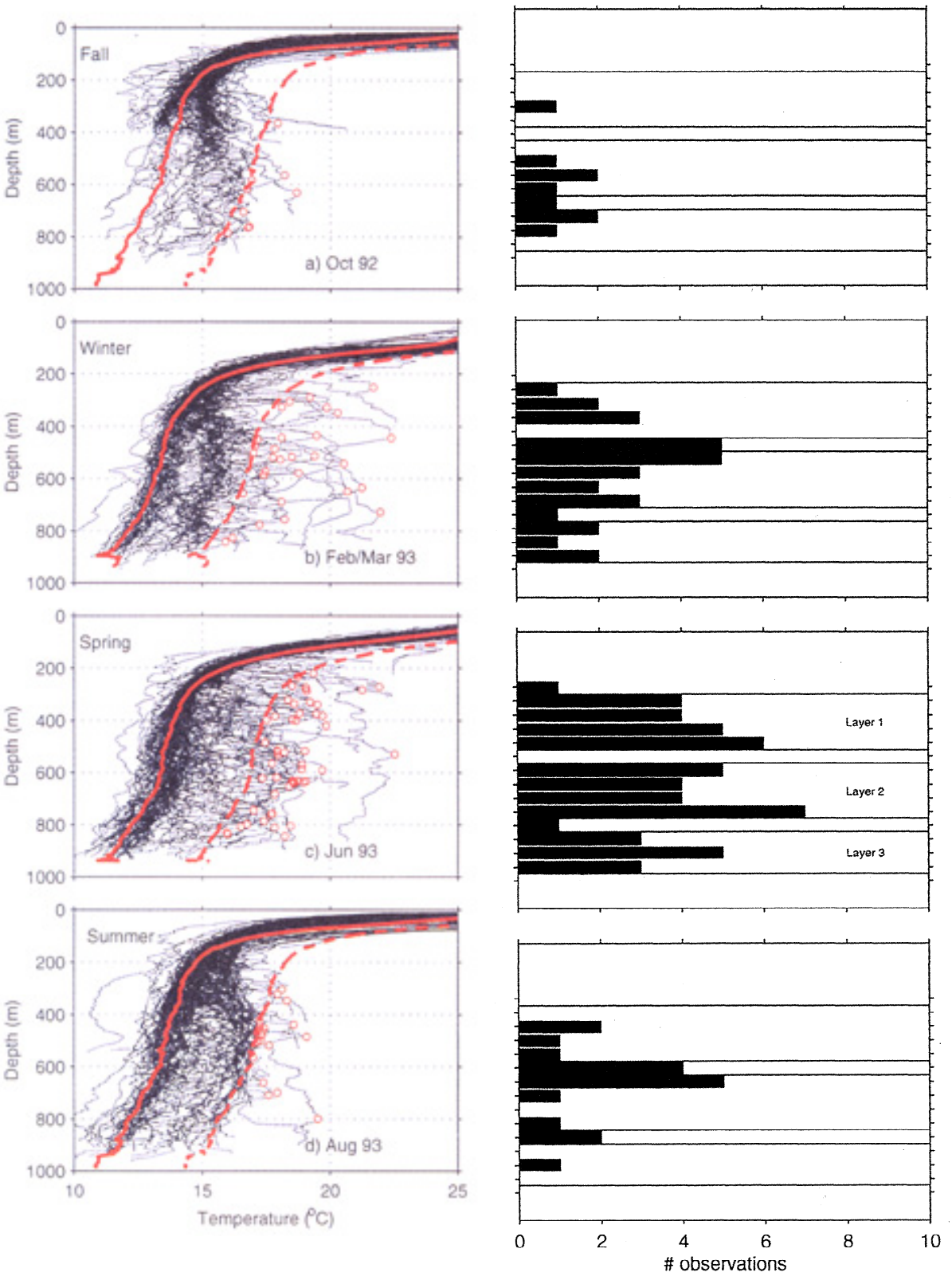

Plate 3. Temperature profiles in the Gulf of Aden from air-deployed expendable bathythermographs (AXBTs) (left-hand plots) and associated histograms of the depth of intermediate temperature maxima (open red circles) for four seasonal surveys in 1992-1993. Solid red line in left-hand plots shows "background" profile, defined as the mean of profiles 48°-50°E, and the dashed red line is 3.5°C warmer and represents the cutoff for recently injected outflow water (see text).

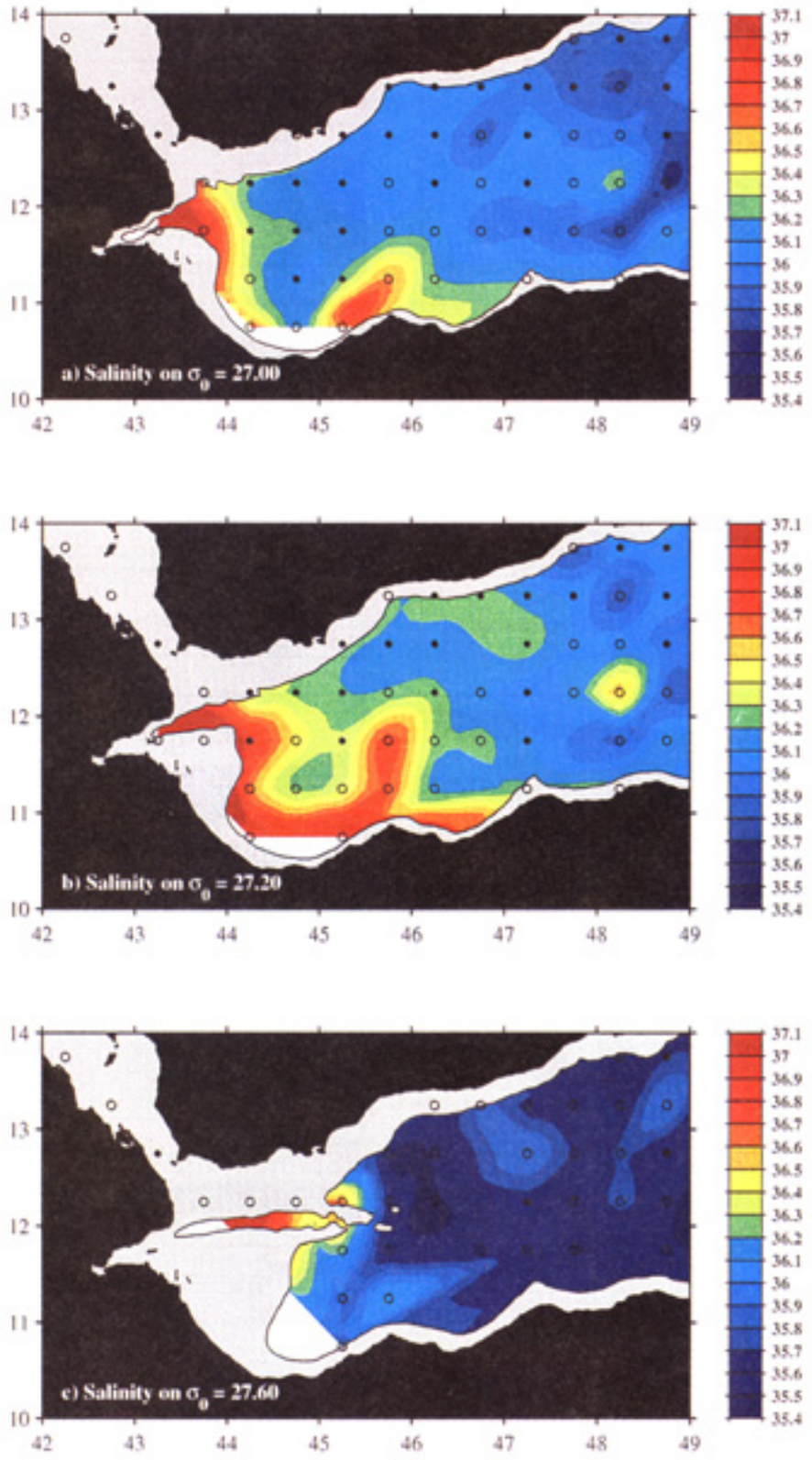

Plate 4. Climatological salinity distributions in the Gulf of Aden on three density surfaces: (a) 27.0, (b) 27.2, and (c) 27.6. Open circles indicate averaging bins, and solid circles show where there were more than five observations in the average.

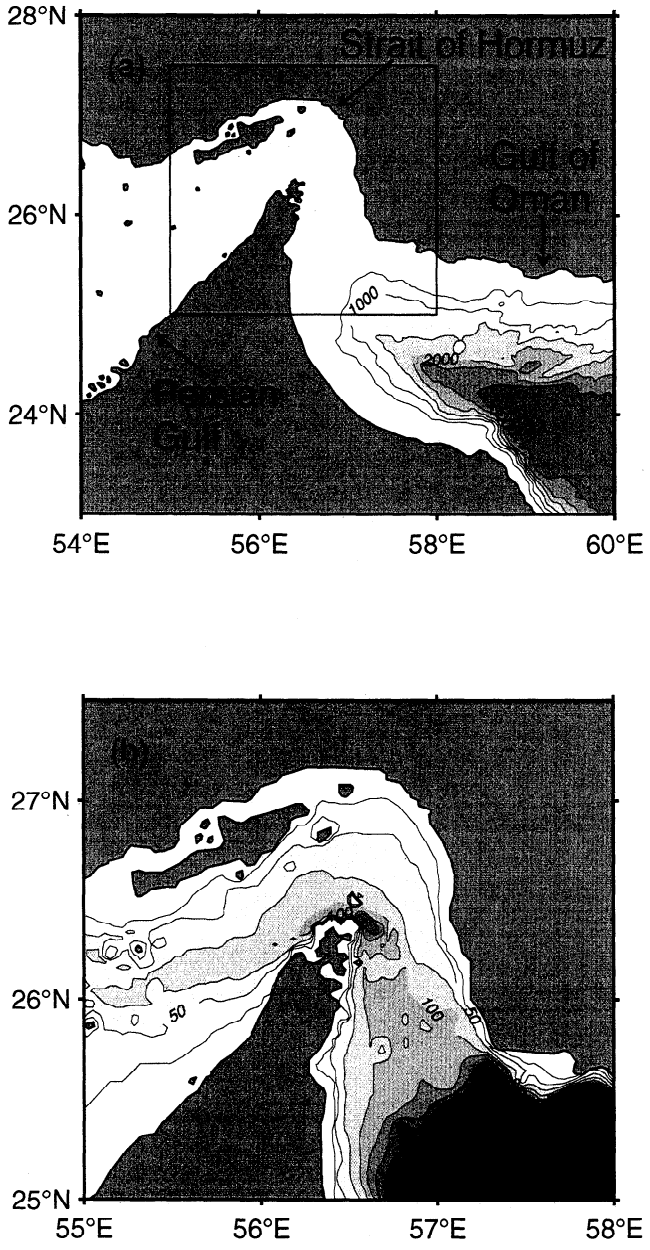

Figure 2. (a) Chart of the eastern Persian Gulf, Strait of Hormuz, and Gulf of Oman. Bathymetry is shaded in 500-m intervals. (b) Expanded view of the Strait of Hormuz and the northwestern Gulf of Oman (area shown by box in Figure 2a). Bathymetry is contoured in 25-m intervals to 300 m.

results from previous studies to provide an improved description of the seasonal variability in bulk properties and initial spreading pathways of the Red Sea and Persian Gulf outflows (sections 3 and 4). This includes analysis of source water properties (before significant entrainment occurs), product water properties (after entrainment is completed), and oceanic water properties. Second, we have used the results from this analysis to estimate the dilution factors due to entrainment for the Red Sea and Persian Gulf outflows and compared them to the four marginal sea outflows of the Atlantic studied by PB94 (section 5). Finally, we have employed the one-dimensional outflow model of PB94, initialized with results from the data analysis, to examine the dynamics of these two outflows (section 6). In particular, we have explored the effects of low latitude, topography, and seasonal variability in source water and oceanic water characteristics in setting the product water properties of RSW and PGW. Results are discussed and summarized in section 7.

2. Data and Methods

Two new data sets that have recently become available were used to describe the bulk properties of the Red Sea and Persian Gulf outflows and the surrounding oceanic environment. The first consists of all the public domain temperature-salinity-depth (TSD) profile data contained in the Master Oceanographic Observations Data Set (MOODS) at the U. S. Naval Oceanographic Office (NAVOCEANO) at Stennis Space Center. The TSD data were obtained from the regions 10°-17°N, 42°-55°E (southeastern Red Sea, BAM Strait, Gulf of Aden, and western Arabian Sea) and 20°-30°N, 47°-65°E (Persian Gulf, Strait of Hormuz, Gulf of Oman, and northwestern Arabian Sea). This data set includes both high-resolution (salinity-temperature-depth (STD) and conductivity -temperature-depth (CTD)) and low-resolution (e.g., bottle) profiles.

A total of 4184 and 2885 TSD profiles were obtained for the Red Sea and Persian Gulf outflow regions, respectively. Since the data originated from a variety of sources and were collected over the years 1923-1996, it was necessary to perform a quality control analysis. The technique outlined by *Curry* [1996] was used, and the reader is referred to that work and to *Alessi et al.* [1999] for details on the quality control procedure. In brief, the TSD data were first grouped into subregions (and in some cases seasons) that exhibited a similar potential temperature-salinity (T-S) relationship. The data were then averaged in density bins to obtain a mean T-S relationship for each subregion, and individual observations > 2.3 standard deviations away from the mean T-S curve were eliminated. This resulted in a rejection of ~3.5% of the observations. As pointed out by *Curry* [1996], this method does not guarantee that all erroneous observations are eliminated, nor that all good data are retained. It is simply an objective, statistical approach to removing observations that have a high probability of being incorrect.

The second data set used in the analysis is made up of ~2800 air-deployed expendable bathythermograph (AXBT) profiles, also obtained from MOODS. It will be shown in sections 3 and 4 that temperature can be used as a tracer of RSW and PGW up to several hundred kilometers away from their respective sources. These profiles extend from the sea surface to nominal depths of 400 m or 800 m. They were collected as part of nine synoptic surveys in the Gulf of Aden and Gulf of Oman conducted over a 2.5 year period from October 1992 to March 1995 (Table 1). Each survey consisted of a grid pattern with nominal station spacing of 35 km. The AXBT data were quality controlled at NAVOCEANO, and a few profiles were subsequently eliminated owing to suspicious data. The accuracy of temperature and depth from the AXBTs is about $\pm$ 0.2°C and $\pm$ 5 m [*Boyd*, 1986].

The number of profiles per survey ranged from 32 to 248 in the Gulf of Aden and 42 to 199 in the Gulf of Oman (Table 1). The 800-m AXBTs were used extensively in the Gulf of Aden owing to the greater equilibrium depth of the RSW. In

Table 1. Summary of NAVOCEANO Air-Deployed Expendable Bathythermograph (AXBT) Surveys

Survey	Start Date	End Date	Number of Days	Number of Profiles		
				400 m	800 m	Total
Gulf of Aden AXBT Surveys						
1	Oct. 11, 1992	Oct. 15, 1992	5	159	51	210
2	March 1, 1993	March 7, 1993	7	87	133	220
3	June 1, 1993	June 6, 1993	6	118	130	248
4	Aug. 21, 1993	Aug. 31, 1993	11	59	157	216
5	Nov. 18, 1993	Nov. 18, 1993	1	9	23	32
6	March 10, 1994	March 12, 1994	3	36	91	127
7	0	0	0	0	0	0
8	Dec. 7, 1994	Dec. 9, 1994	3	44	86	130
9	March 9, 1995	March 13, 1995	5	13	141	154
Gulf of Oman AXBT Surveys						
1	Oct. 7, 1992	Oct. 14, 1992	8	198	1	199
2	Feb. 24, 1993	March 1, 1993	6	199	0	199
3	May 29, 1993	June 9, 1993	12	260	0	260
4	Aug. 12, 1993	Aug. 22, 1993	11	192	0	192
5	Nov. 15, 1993	Nov. 16, 1993	2	108	1	109
6	March 5, 1994	March 12, 1994	8	170	1	171
7	May 27, 1994	May 29, 1994	3	94	0	94
8	Nov. 28, 1994	Dec. 9, 1994	12	168	25	193
9	March 13, 1995	March 13, 1995	1	41	1	42

the following analysis of the Red Sea outflow we will focus on the four surveys of the Gulf of Aden that had >200 AXBT profiles (1-4): They provide the best coverage in the western gulf and make up a quasi-seasonal time series. For the Persian Gulf outflow analysis, we have used surveys 1-8, which all provide good coverage in the western Gulf of Oman.

3. Red Sea Outflow

3.1. Bathymetry and Source Water Characteristics

The Red Sea is a long, narrow marginal sea ~2000 km long and, on average, ~280 km wide [*Morcos*, 1970]. Maximum depths extend to over 2000 m in a narrow central trench. The only significant connection with the open ocean is through the narrow, shallow Bab-al-Mandeb Strait, which extends 150 km from its shallowest point (~160 m) at the Hanish sill to its narrowest point (width ~18 km) at Perim Narrows (Figure 1). The strait then opens up into the western Gulf of Aden. There are two channels leading into the gulf: a main channel extending southeastward from the narrows and a very narrow (width ~5 km) northern channel oriented east-southeastward (Figure 1b) [see, e.g., *Siedler*, 1968] (the northern channel is not resolved in ETOPO2, the 2-min bathymetric data used here, but its location is indicated by an arrow). The channels deepen gradually at first, then rapidly at the northern edge of the narrow, deep (~1800 m) Tadjura Rift, which runs nearly east-west at ~12°N. South of the rift, there is a broad submarine headland which we will refer to as the Tadjura Spur.

Maximum outflow transport of RSW occurs in winter (October-May), when the winds in the southern Red Sea are from the south-southeast. During this time of year, there is a relatively strong two-layer exchange flow through BAM Strait, with the saline, dense RSW flowing out in the lower layer and fresher Gulf of Aden water entering the Red Sea in the upper layer. Minimum outflow transport occurs during summer (June-September), when prevailing winds from the north-northwest drive a surface flow out of the Red Sea, and Gulf of Aden water flows into the Red Sea in an intermediate

Table 2. Parameters Used in T-S Comparisons and Model Simulations

	RS Winter	RS Summer	PG Winter	PG Summer
		Source water properties		
H, m	100	50	45	45
U, m s^{-1}	0.60	0.10	0.17	0.17
W, km	10	10	30	30
Θ, °C	22.9	20.7	21.0	24.0
S	39.9	39.0	40.6	40.0
σ_θ, kg m^{-3}	27.69	27.63	28.77	27.43
		Oceanic Conditions		
Θ, °C	15		22	
S	36.0		36.5	
σ_θ, kg m^{-3}	26.7		25.4	
Oceanic profile location	11.5°N, 45.5°E	11.5°N, 44.5°E	25.5°N, 57.5°E	25.5°N, 57.5°E
		Product Water Properties (Climatological)		
Θ, °C	17.9		21.7	
S	37.5		37.8	
σ_θ, kg m^{-3}	27.2		26.5	

H, height; U, speed; W, width; Θ, potential temperature; S, salinity; σ_θ, potential density.

layer sandwiched between the surface layer and the outflowing RSW layer. Recent current meter and acoustic doppler current profiler (ADCP) observations at the Hanish sill indicate a typical outflow transport of ~0.6 Sv in winter and 0.05 Sv in summer [*Murray and Johns*, 1997]. Typical values for outflow height, width, and velocity were observed to be 100 m, 10 km, and 0.6 m s^{-1} during winter and 50 m, 10 km, and 0.1 m s^{-1} during summer (Table 2). Maximum outflow speeds of >1 m s^{-1} were observed in late February, and outflow transport ceased completely for short periods during summer. Murray and Johns' estimate of the annual mean RSW outflow transport, 0.37 Sv, agrees well with *Siedler's* [1969] often quoted estimate of 0.33 Sv, which is based on the Knudsen relations.

Within the Red Sea, RSW is a nearly isothermal (~22°C), isohaline (~40.5) water mass extending from ~80 m to the bottom [*Maillard and Soliman*, 1986], whose *T-S* characteristics vary little on seasonal or shorter timescales [see, e.g., *Siedler*, 1968; *Quadfasel and Verch*, 1987]. At the northern end of BAM Strait (Hanish sill) the *T-S* characteristics of the outflowing RSW also remain nearly constant throughout the year in spite of the seasonal changes in outflow transport. Using moored CTDs, *Murray and Johns* [1997] found that the *T-S* of the outflowing RSW was 22°-23°C and 40.0-40.6 throughout the 10-month sampling period.

In the numerical simulations which follow, the outflow is started at the southern not northern end of the strait since we anticipate that not much turbulent entrainment occurs along the strait itself because of the weak bottom slope: Depth increases from ~160 m to 250 m over the 150 km between the Hanish sill and the Perim Narrows (average bottom slope of 0.6 x 10^{-3}). Also, the model physics do not include processes that might be important in the narrow strait, e.g., hydraulic control. Thus we define the "source" of RSW at the narrows and must determine the *T-S* characteristics at this location from the historical hydrographic data. The outflowing RSW does mix somewhat with the overlying Gulf of Aden water as it transits the strait [*Siedler*, 1968; *Maillard and Soliman*, 1986], and as a result, the *T-S* characteristics (but probably not transport) of RSW at the narrows are different from those at the sill.

Plate 1a shows the locations of historical hydrographic stations near the narrows that extended deeper than 100 m (i.e., deep in the channel), and Plates 1b-1d show the salinity, potential temperature, and potential density of these data as a function of day of year. The large variability for a given time of year mostly reflects the vertical property gradients within the deep channel (see, e.g., *Murray and Johns* [1997] and discussion below). Maximum salinities are generally > 39.5 in winter (November-June) and < 39.2 during summer (Plate 1b). Potential temperature of the most saline observations (arbitrarily chosen in Plates 1b-1d as S > 39, indicated by open circles) is also lower in summer, generally < 21°C compared to 22°-24°C in winter (Plate 1c).

A *T-S* diagram of these data (those deeper than 100 m) illustrates the distinction between the summer and winter regimes (Plate 1f). In winter (blue dots), temperature increases slightly upward (and salinity decreases rapidly), while in summer (red dots), temperature decreases upward owing to the presence of cool Gulf of Aden water flowing into the Red Sea above the RSW. Typical source water properties in the two seasons, 22.9°C and 39.9 for winter and 20.7°C and 39.0 for summer, were obtained by averaging the observations that were in the homogeneous RSW layer (Plate 1e). This amounted to averaging the most saline observations for each season, S > 39.50 for winter and S > 38.75 for summer (see vertical lines in Plate 1e). Note that the winter *T-S* characteristics are close to those observed year-round at the Hanish sill, indicated by the square in Plate 1f. The average depth of the most saline winter and summer observations was 200 m and 250 m, respectively. *Maillard and Soliman* [1986] observed a similar seasonal change in source water temperature near the narrows, from 22.5°-23.0°C in June-July 1982 (late winter/early summer) to 20.5°-21.0°C in September-October of the same year (late summer). From these results it appears that the RSW entering the Gulf of Aden is cooler and fresher in summer not because of variations in the Red Sea but rather because of mixing in BAM Strait with the seasonally varying Gulf of Aden water flowing into the Red Sea above it.

3.2. Product Water Characteristics

Previous hydrographic observations in the western Gulf of Aden have shown evidence that RSW equilibrates at several depths, although the exact depths and their seasonal variability have not been clearly established owing to the lack of high-resolution synoptic observations along the path of the equilibrated outflow water (product water). Composite images of the vertical distribution of RSW in the gulf (i.e., where observations have been spatially and/or temporally averaged) reveal two main equilibrium levels: the classical one centered at ~600 m, and σ_θ = 27.2 and a deeper layer at 1000-1200 m and σ_θ = 27.65 [Siedler, 1968; Fedorov and Meshchanov, 1988]. These two layers are also apparent in the western half of average temperature and salinity sections from the NAVOCEANO hydrographic database (Plate 2). These sections were produced by (isopycnally) averaging all the hydrographic data in 0.5° squares, then choosing a set of node points along the western and southern boundaries of the gulf, the preferred spreading pathway of the equilibrated outflow water (see section 3.3). The maximum T-S of the equilibrated RSW is 17.9°C and 37.5 for the classical layer and somewhat cooler, ~16.5°C, with the same salinity for the deeper layer (note that although the first six node points are all shown shallower than 1000 m, their associated averaging boxes extend into deeper water). In the eastern half of this section, RSW is concentrated in a single thick layer centered at the classical equilibrium level, with the salinity maximum centered at ~27.2 σ_θ.

The limited number of synoptic hydrographic observations in the western gulf indicate a more complex vertical structure [Siedler, 1968; Maillard and Soliman, 1986; Beal et al., 1999]. On the basis of temperature profiles alone, Maillard and Soliman identified several layers of equilibrated RSW above 1000 m that were only apparent (as intermediate temperature maxima) in winter and spring. Below 1000 m they observed a temperature maximum in both spring and summer. On the basis of these observations, Maillard and Soliman suggested that the intermediate layers (< 1000 m) of RSW were "fed" only during winter and that the deep layer (> 1000 m) was supplied year-round.

The NAVOCEANO hydrographic data are not of sufficient vertical resolution to identify possible multiple layers of RSW that might exist above 1000 m. However, T-S diagrams of the winter and summer data indicate that there is highly saline (S > 37) RSW above 1000 m in both seasons (top right corner of Figures 3a and 3b), suggesting that RSW does equilibrate above 1000 m in summer as well as winter. In section 3.1 it was shown that the Red Sea source water is cooler in summer, and in the discussions to follow, we show that the product waters are cooler as well. This may make it more difficult (but not impossible; see below) to detect these layers in summer with temperature alone and may have led Maillard and Soliman [1986] to conclude (based on just a few stations) that RSW does not equilibrate above 1000 m in summer.

The repeated AXBT surveys in the Gulf of Aden provide more details, at least on the temperature structure of the product water. Plates 3a-3d show the temperature profiles for the area 43°-50°E from the four well-sampled AXBT surveys, which together make up a quasi-seasonal time series (see Table 1). The solid red line in each panel shows the mean of profiles from 48°-50°E and represents the "background" profile for each survey. In October 1992 (Plate 3a), there were very few deep AXBTs in the eastern gulf, so the mean profile from August 1993 is displayed instead. Since the AXBTs only reach a maximum depth of 800-900 m, we focus here only on the RSW layers above 1000 m.

These temperature profiles appear to separate into three types, especially evident in Plate 3b: (1) profiles characterized by strong interleaving below 200 m and/or the warmest temperatures, (2) profiles with less interleaving and maximum temperatures between the highly interleaved profiles and the background profile, and (3) profiles where temperature decreases monotonically with depth. We interpret the first type as representing the most recently injected outflow water, the second type as representing partially mixed outflow water from the previous winter's injection, and the third type as representing the "background" profiles. The distinction between the second and third types is variable and most apparent in Plates 3b and 3d.

Focusing on the first type of profile, there is evidence of recently injected, equilibrated outflow water in all four surveys/seasons, indicated by intermediate temperature maxima. The product water temperature is higher in winter and spring compared to summer and fall. The mean temperature of the intermediate temperature maxima more than 3.5°C warmer than the background temperature (red circles in Plates 3a-3d) is 18.7 (winter), 18.5 (spring), 17.7 (summer), and 17.1°C (fall). The temperature maxima are found at multiple equilibrium depths in each survey, and there is no apparent seasonal trend in equilibrium depth. The right-hand plots in Plate 3 show the vertical distributions of these temperature maxima. In fall and summer, there are fewer temperature maxima, consistent with the low outflow transport at that time of year. Otherwise, there are clusters of maxima at several depths, most clearly defined in the June (spring) survey, when there were concentrations of temperature maxima in three layers: 225-425 m (layer 1), 475-675 m (layer 2), and 725-875 m (layer 3). The small vertical scale of these layers emphasizes the need for high vertical resolution observations to detect them and describe their basic structure.

Summarizing the product water characteristics of the Red Sea outflow, in a climatological sense, there are two main layers of equilibrated RSW in the western Gulf of Aden, the classical one at ~600 m, with θ = 17.9°C and S = 37.5, and a cooler, denser layer (θ = 16.5°C) below 1000 m. Synoptically, the classical layer appears to be made up of thin (thickness ~100 m) salinity-temperature maxima which are only apparent in high-resolution profiles in the western gulf. These layers are present year-round, are found from 200m to 800 m, and are cooler in summer compared to winter (~17°C compared to ~19°C). There is some evidence of preferred equilibrium depths at certain times of the year.

There are two basic hypotheses that could explain the presence of these multiple layers: (1) different mixing histories along the two (or possibly more) channels at the exit of BAM Strait, as has been suggested by Fedorov and Meshchanov [1988], and (2) seasonal variability in source water characteristics or in the oceanic properties. The existence of multiple layers within a single AXBT survey lends support to the former. In section 6, we will explore these hypotheses using the outflow model.

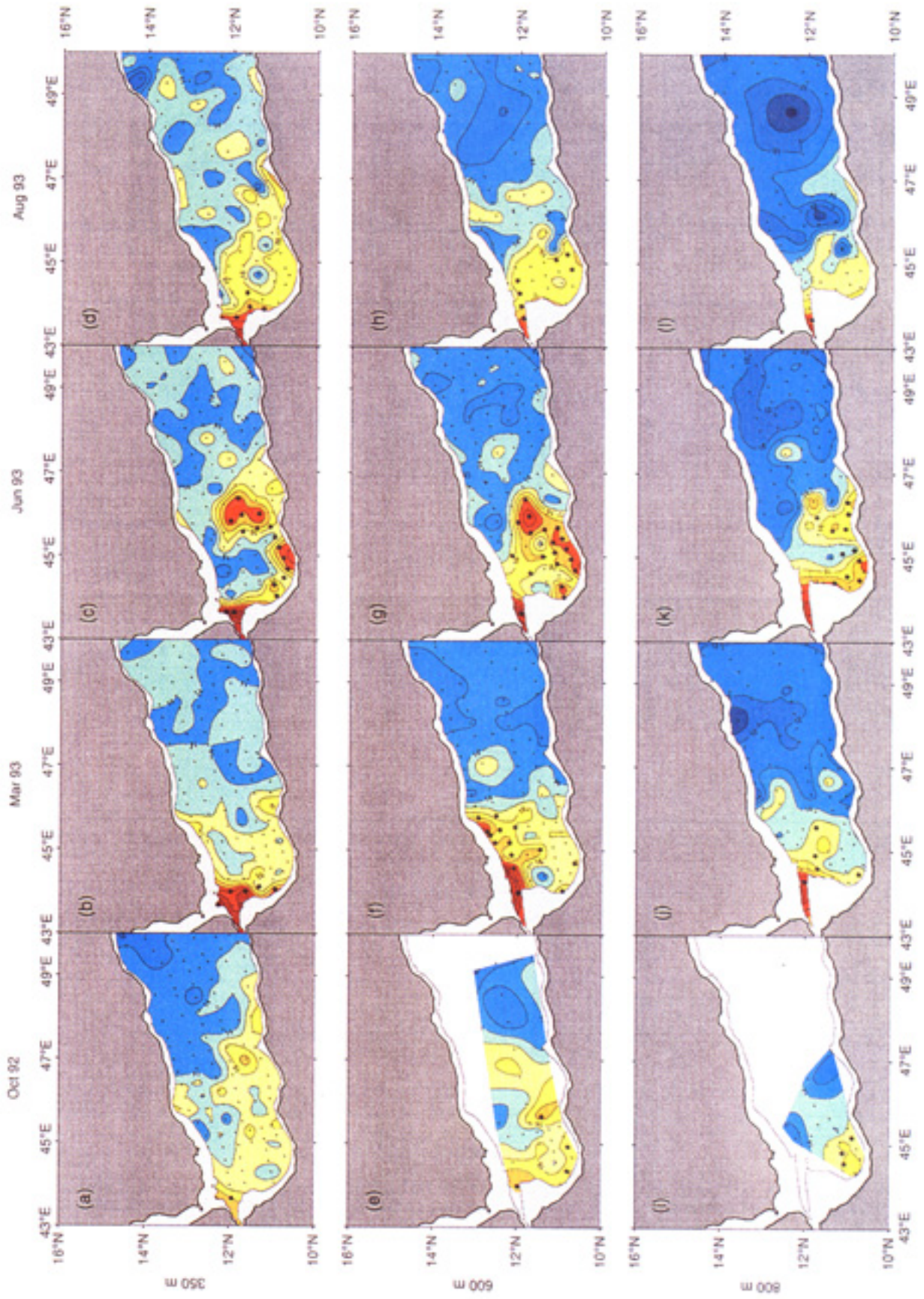

Plate 5. Synoptic distributions of temperature at three depths for the four seasonal surveys. Contour interval is 1°C, and the small dots show the station locations. Asterisks indicate the locations of intermediate temperature maxima at the corresponding depths.

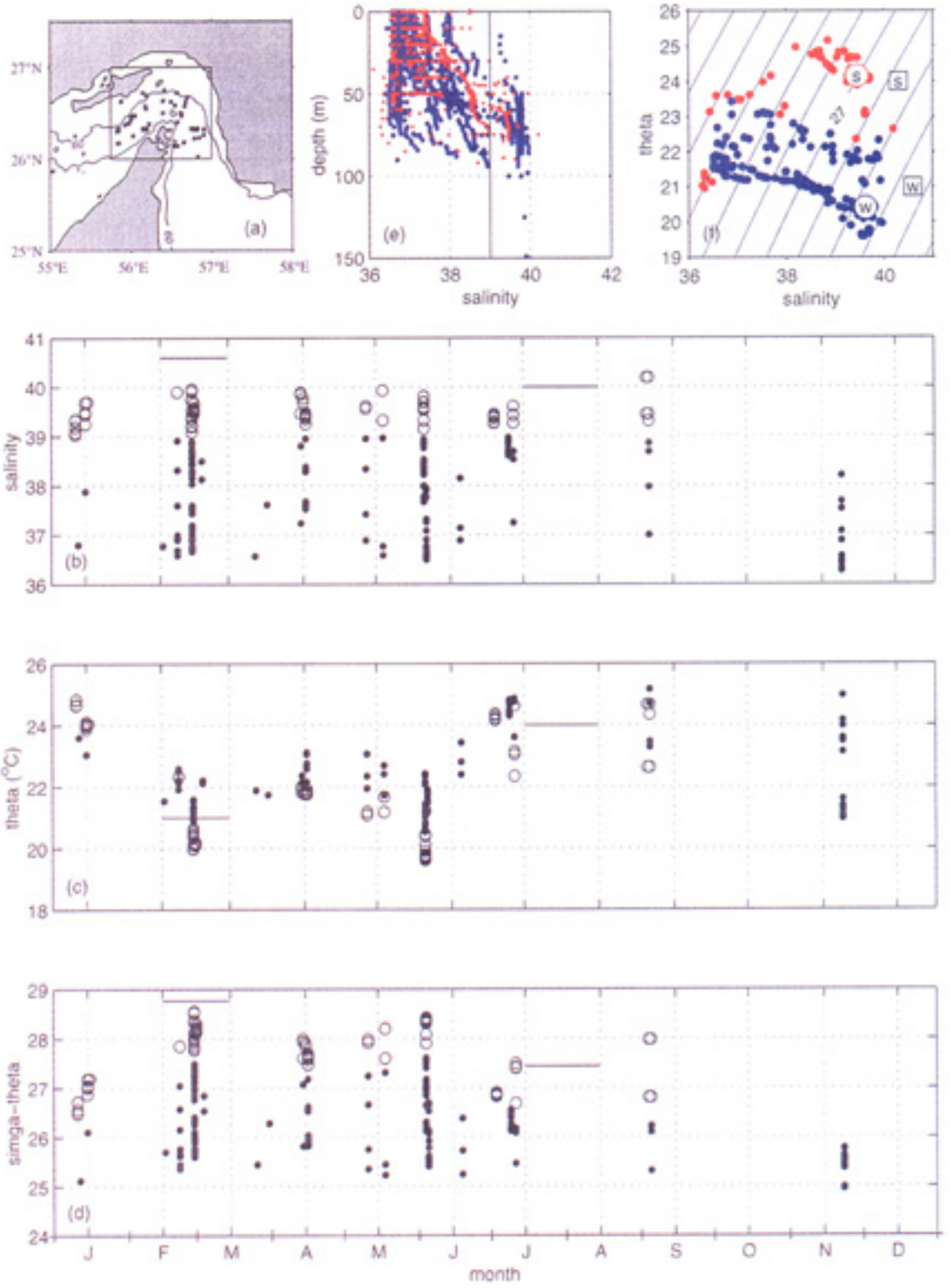

Plate 6. (a) Positions of hydrographic observations deeper than 60 m in the Strait of Hormuz. (b-d) Salinity, potential temperature, and potential density of these observations as a function of day of year. The circles indicate observations with $S > 39$, and horizontal lines show typical winter and summer values from a moored conductivity-temperature-depth (CTD) in the strait. (e) Salinity as a function of depth for all observations in the strait for both winter (blue) and summer (red). The vertical line indicates the cutoff used to compute the average T-S characteristics shown in (Plate 6f). (f) T-S diagram of observations deeper than 60 m in summer (red) and winter (blue). Circles indicate mean values for the Persian Gulf outflow based on the hydrographic measurements, and the squares indicate mean values based on the moored measurements.

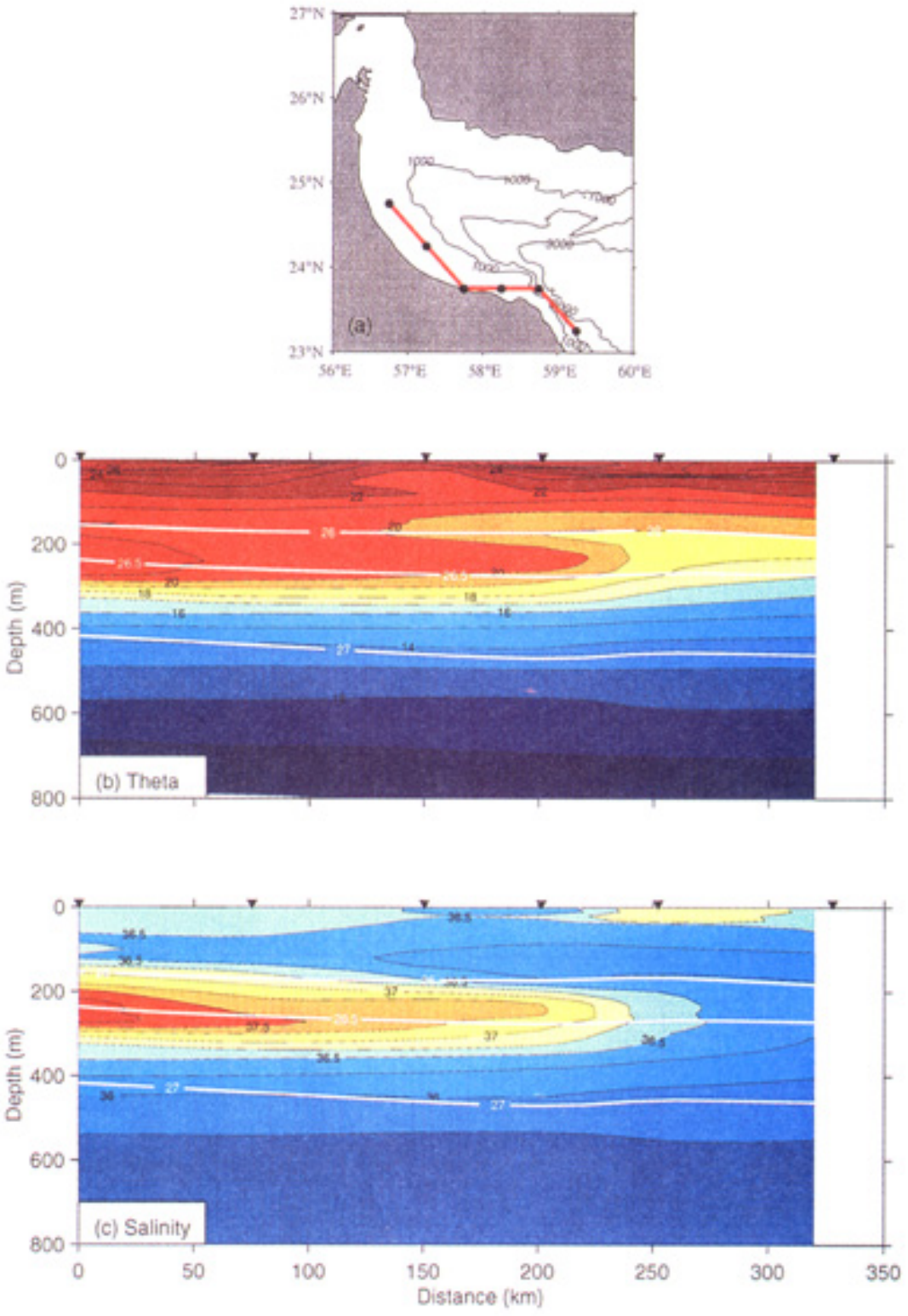

Plate 7. (a) Location of section along path of Persian Gulf outflow. Climatological distributions of (b) potential temperature and (c) salinity along the section shown in (Plate 7a) obtained by averaging the NAVOCEANO hydrographic data in 0.5° squares. Three potential density contours are superimposed.

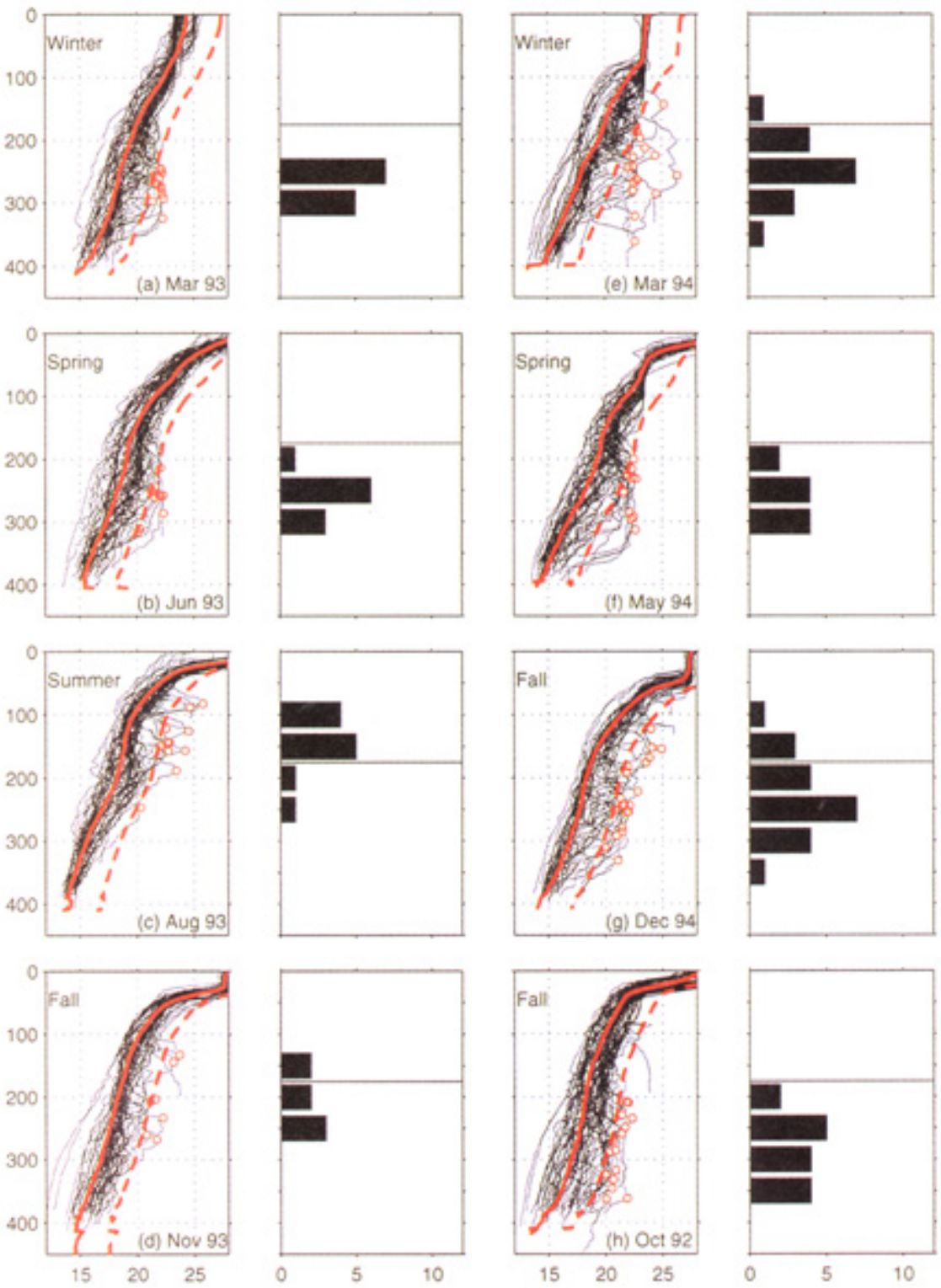

Plate 8. AXBT temperature profiles in the Gulf of Oman for eight synoptic surveys in 1992-1994 and associated histograms showing depth distributions of intermediate temperature maxima (red circles) more than 3.0°C warmer than the background. The "background" profile for each survey is shown by solid red line, and the dashed red line is 3.0°C warmer and represents the cutoff for recently injected outflow water (see text). Plots are arranged by season.

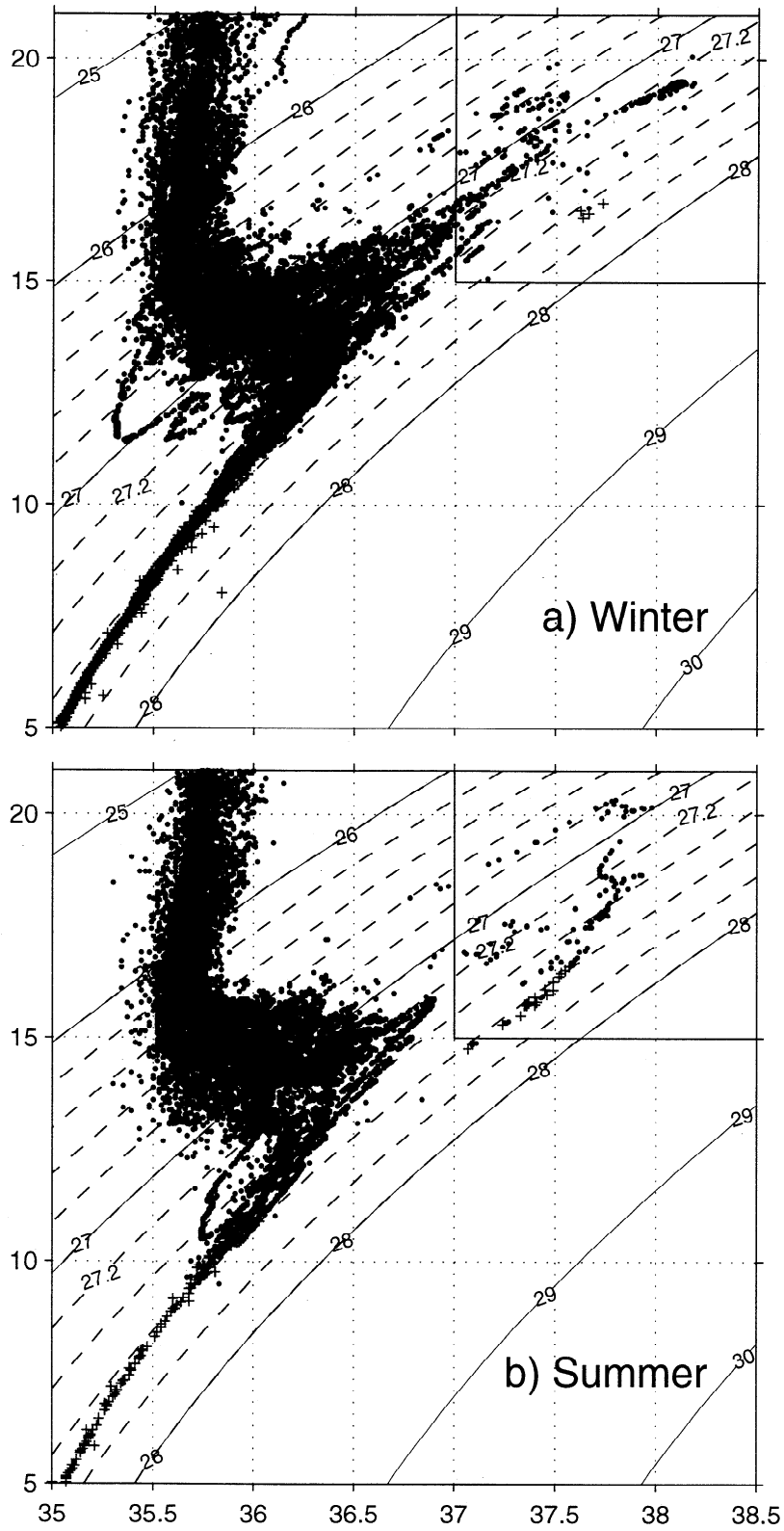

Figure 3. *T-S* diagrams for hydrographic observations in the western Gulf of Aden during (a) winter and (b) summer. Dots indicate observations shallower than 1000 m, and pluses indicate observations > 1000 m.

3.3. Spreading Pathways of Red Sea Product Water

Plate 4 shows the average salinity distributions on three of the density surfaces shown in Plate 2: σ_θ = 27.0 (~400 m), 27.2 (~600 m) and 27.6 (~1000 m). On the upper two density surfaces the highest-salinity water extends from the strait first southward then eastward along the continental slope in a narrow vein to ~46°E. On the 27.6 density surface the most saline water appears to be confined to the Tadjura Rift. Plate 5 illustrates the variability in the synoptic distribution of outflow water based on the four AXBT surveys described above. Temperature at three depths is contoured, and the locations of the warm temperature inversions in layers 1-3 (from Plate 3) are indicated by asterisks to show the spreading pathways of the most recently injected outflow water.

In layer 1 (350 m) (Plates 5a-5d) the most recent outflow water was found along the western and/or southern boundaries of the gulf in all four surveys and in a large, ~100-km-diameter eddy centered at ~46°E in the June 1993 survey (Plate 5c). The vein of warm water along the slope does not always appear continuous (e.g., Plate 5c). The greatest longitudinal extent of recently injected outflow water was observed in the June survey, when temperatures warmer than 18°C were observed out to 46.5°E. This is just after the season of maximum outflow transport. In layer 2 (600 m) (Plates 5e-5h) warm outflow water is also observed along the western and/or southern slopes of the gulf and in the large eddy in the June survey (Plate 8g), but the continuity of the boundary vein is less clear. Also, there is a concentration of outflow water along the northern edge of the gulf west of ~46°E in the late winter survey (Plate 5f), possibly reflecting the importance of the northern channel as a significant source of outflow water to this layer. There are also some warm inversions due east of the rift in the late winter and spring surveys, suggestive of a direct pathway from the rift into midgulf. Note also the relatively homogeneous pool with temperatures 16°-17°C west of ~46°E in the summer survey (Plate 5h). This represents the partially mixed outflow water that is distinct from the "background" water that is found farther east, as also seen in Plate 3d. In layer 3, there is evidence of a spreading pathway along the boundary (Plate 5k) and eastward from the rift (Plate 5j).

These temperature and salinity distributions indicate that equilibrated RSW spreads away from BAM Strait primarily in a narrow vein along the western and southern boundaries of the gulf. There is also some evidence of an intermittent path due east from Tadjura Rift. The boundary vein of RSW does not appear to extend east of 46.5°E. These results are suggestive of a narrow boundary current that transports the recently injected outflow water along the continental slope of Africa for several hundred kilometers, much like the Mediterranean Undercurrent in the Gulf of Cadiz [see, e.g., *Ambar and Howe*, 1979a, b]. The patchiness seen here may be real, resulting from instability of a possible boundary current, or it may be the result of the relatively coarse spatial resolution of our data. The apparent termination of this spreading pathway near 46°E could be related to the presence of the cape there, which may cause separation of the boundary current as has been observed for the Mediterranean Undercurrent at Cape St. Vincent [*Bower et al.*, 1997].

4. Persian Gulf Outflow

4.1. Bathymetry and Source Water Characteristics

In contrast to the Red Sea, the Persian Gulf is extremely shallow, with a maximum depth of ~100 m in a central basin and an average depth of only 35 m. The Strait of Hormuz is generally wider and shallower than BAM Strait: 57 km wide overall at its narrowest point (although the central channel is about half as wide) and with a sill depth of ~80 m (Figure 2b). It opens onto the continental shelf in the northwestern Gulf of Oman.

High evaporation rates (1.5-5 m yr^{-1} [*Chao et al.*, 1992]) and the shallowness of the Persian Gulf lead to the formation of very saline, dense water, having maximum salinities as high as 57 in shallow estuaries along the southern coast [*John et al.*, 1990], although maximum salinities of PGW over most of the gulf are 40.0-40.5 [*Brewer et al.*, 1978; *Chao et al.*, 1992]. Densification of the water in the Persian Gulf drives an exchange flow through the Strait of Hormuz, where fresher Indian Ocean water flows into the Persian Gulf at the surface on the northern side of the strait, and the saline PGW exits at the bottom on the south side of the strait [*Brewer et al.*, 1978; *Horton et al.*, 1994]. *Ahmad and Sultan* [1991] employed the Knudsen relations to estimate the annual mean PGW outflow transport at 0.17 Sv. Recent observations from an ADCP moored in the Strait of Hormuz indicate no strong seasonal variations in outflow transport and an annual mean of ~0.20-0.25 Sv (W. Johns, personal communication, 1998).

The seasonal variability in the *T-S* characteristics of the Persian Gulf source water is not documented in the literature, so we rely on the historical hydrographic data from the region and recent observations obtained by W. Johns from a CTD moored with the ADCP in the strait. Plate 6a shows the locations of all observations in the NAVOCEANO database deeper than 60 m in the Strait of Hormuz. Plates 6b-6d show the salinity, temperature, and density in the channel as a function of time of year. Typical winter and summer salinity, temperature, and density values observed at 100 m with the moored CTD are indicated by horizontal lines (W. Johns, personal communication, 1998).

As in the Red Sea case, there is considerable variability in hydrographic properties for a given time of year. This is partly due to vertical gradients in the deep channel but also to horizontal gradients. The Strait of Hormuz is wider than BAM Strait, and the higher latitude means that the Persian Gulf outflow is banked up against the southern side of the strait [*Horton et al.*, 1994]. The *T-S* characteristics of the most saline observations (say $S > 39$, circles in Plates 6b-6d), however, give an indication of the seasonal variability in source water properties. There seem to be more observations with salinity > 39.5 in the first half of the year compared to the second half (Plate 6b), although the latter time period has fewer observations overall, and the single highest salinity observation, 40.2, was observed in the second half of the year. This tendency, however, agrees with the Johns moored observations, which show a winter salinity of 40.6 and a slightly lower summer value, 40.0. Curiously, all but one of the hydrographic observations are < 40: This is probably due to the fact that the moored CTD was deeper in the channel than most of the hydrographic observations (see below).

Both the hydrographic observations and the Johns measurements reveal a strong seasonal cycle in temperature (Plate 6c). The most saline water is cooler by several degrees during February-June (~19°-22.5°C) compared to July-January (22°-25°C). This matches the observations of Johns: 21°C in winter and 24°C in summer. This variation is consistent with the seasonal heating cycle over the Persian Gulf [*Horton et al.*, 1994]. The winter decrease (increase) in outflow temperature (salinity) results in a substantial winter-summer difference in outflow density of almost 1.3 kg m^{-3} based on the Johns measurements [Plate 6d]. This can also be seen in the *T-S* diagram for the hydrographic observations (Plate 6f). Typical winter and summer *T-S* values based on the hydrographic data were obtained by averaging summer and winter observations with $S > 39$. The result is 20.4°C and 39.6 for winter and 24.2°C and 39.4 for summer. The average depth of these observations was ~75 m, which is 25 m shallower than the Johns observations. Since the latter were made well within the outflowing layer, we will use them in the Persian Gulf outflow model simulations discussed below.

4.2. Product Water Properties

Plate 7 shows potential temperature and salinity sections along the main pathway of the equilibrated Persian Gulf product water (see below). At the node point closest to the source (0 km), temperature and salinity maxima, with peak values of 21.7°C and 37.8, are observed at ~225 m and 26.5 σ_θ.

Unfortunately, the NAVOCEANO hydrographic data are not sufficient to investigate seasonal variations in the product water characteristics: There are just a handful of profiles from the summer months [*Alessi et al.*, 1999]. The repeated AXBT surveys, however, can be used to examine the seasonal variability in equilibrium depth and product water temperature. Plate 8 shows the AXBT profiles for each survey. In this case, there are at least two surveys for each season except summer. There are basically two types of temperature profiles: those with temperature inversions, indicative of the recently injected outflow water, and those where temperature decreases monotonically with depth (at least below the mixed layer). We have identified intermediate temperature maxima more than 3°C warmer than the background (defined here as the mean of profiles from 58°-60°E) and histograms indicating the vertical distribution of these maxima are also shown in Plate 8.

In most of the surveys the temperature maxima are found from 200 m to 350 m, with the most usually at 250 m. The mean temperature and depth of the maxima deeper than 175 m across all surveys are 21.9°C and 260 m, respectively, which are similar to the results from the hydrographic data. There is as much variability in the temperature of these maxima within the same season as there is between seasons (e.g., Plates 8a and 8e). The most obvious difference between surveys in the outflow profiles is that in the one summer survey (Plate 8c), there are only a few warm temperature maxima below 200 m and a number of much warmer maxima (T = 23°-26°C) between 75 m and 200 m. Note that this is close to the source water temperature in summer/fall, 24°C (see Plate 6). These shallow warm product waters seem to occur mostly in summer/fall compared to winter/spring. In section 6 we will investigate the possibility that the shallower equilibrium depths are the result of the lower source water density during summer and fall.

4.3. Spreading Pathways of Persian Gulf Product Water

In Plate 9 we show the mean distribution of salinity on the 26.5 σ_θ surface (mean depth ~250 m) based on the NAVOCEANO hydrographic data. There is clear evidence of a vein of saline water following the upper continental slope along the western and southern boundaries of the Gulf of Oman. Maximum salinity along this vein is ~38. Plate 9 (and Plate 7) represents the salinity distribution for the months February-June, when the vast majority of the observations were made. This corresponds to our winter season.

Plate 10 shows the synoptic temperature distributions in the Gulf of Oman at the most common equilibrium depth, 250 m, from the eight AXBT surveys, arranged by season, as in Plate 8. Superimposed are the locations of temperature maxima > 3°C warmer than the background (asterisks are for maxima deeper than 175 m, and circles around station dots are for shallower). The clearest evidence of a boundary vein of warm (saline) outflow water like that seen in Plate 9 is found in the two winter surveys (Plates 10a and 10e): Note the continuity of the 21°C isotherm parallel to the boundary. The deeper temperature maxima (asterisks) are also found along this path. There are patches of warmer water and temperature maxima in midgulf, suggesting that recently injected outflow water can be advected off the slope and into the interior.

In the remaining seasons the temperature distribution is more patchy. In the two spring surveys (Plates 10b and 10f) the warmest temperatures are still found along the western and southern boundaries of the gulf but in large, isolated blobs rather than in continuous, narrow veins. In the one summer survey (Plate 10c) the whole gulf is much cooler at this depth, and there are no observations warmer than 19°C. Finally, in fall (Plates 10d, 10g, and 10h) the temperature and maxima distributions are quite patchy, with some concentration along the western and southern boundaries. When the shallow temperature maxima are present, they seem to be clustered in the northwestern corner of the gulf, with a few observations along the western boundary (Plates 13c, 13e, 13g, and 13h).

5. Comparison to Other Marginal Sea Outflows

In Figure 4 we have plotted the change in T-S properties from the source water to the product water in the Red Sea and Persian Gulf outflows and in four other overflows treated by PB94. The arrows begin on the source water T-S and terminate on the product water T-S. The source and product water properties were taken from PB94 for the Weddell overflow from the Filchner Depression, Denmark Strait, Iceland Scotland Ridge, and the Mediterranean overflows. The Red Sea and Persian Gulf source water properties represent winter conditions and were taken from the NAVOCEANO hydrographic data and the Johns mooring, respectively. We focus on the winter conditions because in the Red Sea case this is when the highest outflow transport occurs and in the Persian Gulf case this is the season for which we have the best estimate of the oceanic profile. Product water properties were taken from the climatological water property

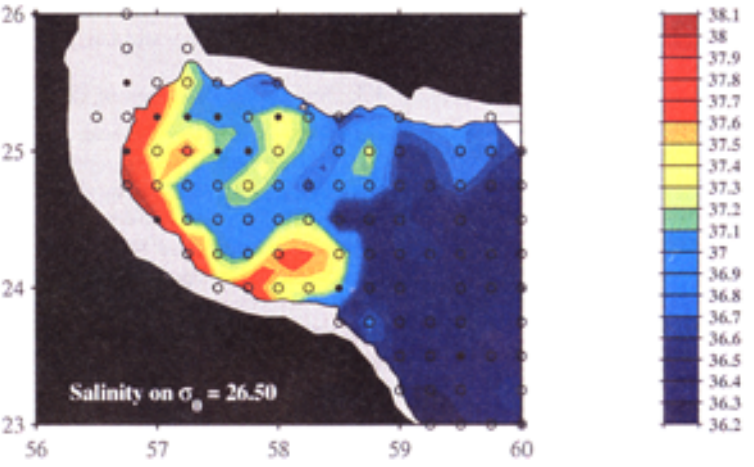

Plate 9. Climatological salinity distribution on the 26.5 potential density surface from NAVOCEANO hydrographic data.

distributions, and the oceanic values represent means for the depth range over which the outflows descend (Table 2). The shaded areas under the Red Sea and Persian Gulf arrow heads give an indication of the variability in product water T-S based on the hydrographic and AXBT data.

One notable feature of this diagram is the striking difference between the source characteristics of the tropical and subtropical overflows (Red Sea, Persian Gulf, and Mediterranean) and the high-latitude overflows. The former are relatively warm and salty, while the latter are cold and fresher. This is because the densification of waters in lowlatitude and midlatitude marginal seas occurs mainly because of an increase of salinity due to an excess of evaporation over precipitation rather than due to cooling. This, of course, reflects the equator to pole variation in air-sea heat flux and fresh water flux.

A second major difference is that the low-latitude and mid-latitude overflow waters undergo much larger changes in density from source to product than do the high-latitude overflows; the Persian Gulf water changes by ~2 kg m^{-3}, the Mediterranean water changes by ~1 kg m^{-3}, and the Red Sea water changes by almost 0.5 kg m^{-3}. For the three high-latitude overflows the corresponding change is 0.1 kg m^{-3} or less. The large changes in density arise mainly because the lowlatitude and midlatitude overflows start at comparatively shallow depths of < 300 m (sill depth) and at sites where there is a well-developed main thermocline. This results in the entrainment of oceanic water (indicated approximately on the *T-S* diagram for the Persian Gulf and Red Sea cases by the shaded circles) that is considerably less dense than the source water. The Red Sea product water characteristics lie ~60% of the distance between the source and oceanic end-members, suggesting a 2.5-fold increase in outflow transport due to entrainment. For the Persian Gulf case, the product water characteristics are ~75% of the distance, indicating a fourfold transport increase. The former is similar to the Mediterranean outflow (PB94), while the latter is significantly greater than for any of the Atlantic outflows. The reason for this will be explored further in section 6.

6. Numerical Simulations

One of the most striking differences between the Red Sea, Persian Gulf, and Mediterranean outflows compared to the other marginal sea outflows discussed above is the large density change between source and product water, suggesting that the former undergo more entrainment and/or entrain water that is much less dense. In this section we use the outflow model of PB94 to further investigate effects of entrainment as well as the dynamical character of the Red Sea and Persian Gulf outflows. The goal here is not to test the model, we do not have the high-resolution hydrographic data to do that as well as was done by PB94, rather it is to identify the main physical processes that determine downstream evolution of the Red Sea and Persian Gulf outflows and investigate the effects of low latitude, topography, and seasonal variability in source water and oceanic characteristics on product water properties.

6.1. Model Description

The reader is referred to PB94 for a detailed description of the outflow model used here. In brief, the outflow is modeled as a single-layer, density-driven bottom current with width W and height H that enters a stratified, open ocean environment. The outflow source water and oceanic properties are assumed to be steady over the time it takes for the outflow to reach equilibrium in the oceanic environment, less than a few days, and the ocean is assumed to be at rest and infinite in extent. Mixing is modeled as an entrainment process that impacts the outflow dynamics. The momentum equation for the outflow is

$$\mathbf{U}\cdot\nabla\mathbf{U}+\mathbf{f}\times\mathbf{U}=g\delta\rho\nabla D/\rho_r-\boldsymbol{\tau}_b/\rho_r H-E\mathbf{U}/H, \qquad (1)$$

where $\mathbf{U}$ is the outflow velocity (horizontal component only), $\mathbf{f}$ is the Coriolis parameter, g is the acceleration due to gravity, $\delta\rho$ is the density difference between the outflow and the oceanic water, D is the bottom depth, ρ_r is the reference density, $\boldsymbol{\tau}_b$ is the bottom stress, and E is the entrainment velocity. Thus the acceleration of the outflow caused by

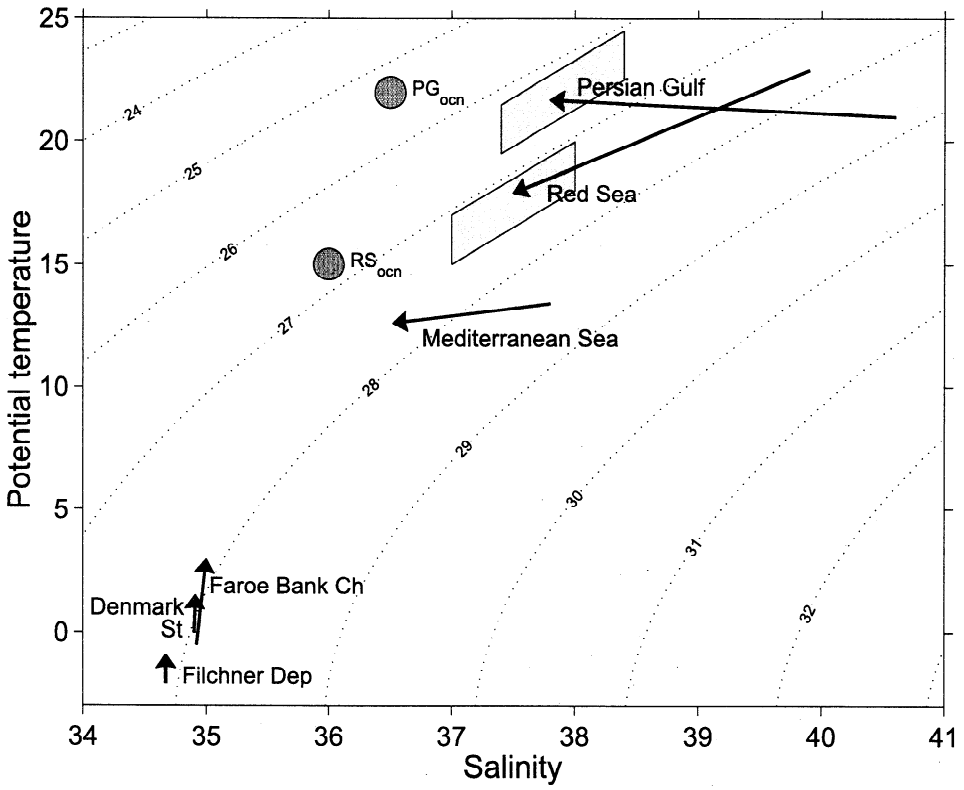

Figure 4. *T-S* diagram showing transformation of outflow water characteristics from source (arrow tail) to product (arrow head) for Red Sea outflow, Persian Gulf outflow, and four other oceanic outflows. The shaded areas under the Red Sea and Persian Gulf arrow heads give an indication of the observed variability in product water *T-S* characteristics. See text for explanation.

Coriolis and buoyancy is opposed by the retarding bottom and entrainment stresses. The heat and salt balances are

$$\mathbf{U}\cdot\nabla\Theta = -E\delta\Theta/H \qquad \mathbf{U}\cdot\nabla S = -E\delta S/H \tag{2}$$

and the continuity equation is written as

$$\mathbf{U}\cdot\nabla H = E - H\mathbf{U}\cdot\nabla W/W - H\nabla\cdot\mathbf{U}. \tag{3}$$

The entrainment velocity, bottom stress, and outflow width are parameterized in terms of known quantities as follows:

$$E = U(0.8 - 0.1\,Ri)/(1+5\,Ri) \quad \text{if} \quad Ri \le 0.8\,(F \ge 1)$$
$$E = 0 \quad \text{otherwise} \tag{4}$$
$$Ri = g\delta\rho H/\rho_r U^2 = F^{-2}.$$

Here Ri is the layer Richardson number, also expressed in terms of F, the layer Froude number. The bottom stress is parameterized by the usual quadratic form,

$$\boldsymbol{\tau}_b = \rho_r C_d U\mathbf{U}, \tag{5}$$

where C_d is the drag coefficient. The rate of widening is specified according to

$$(\mathbf{U}\cdot\nabla W)/U = \beta, \tag{6}$$

where β is determined from the bathymetry if the outflow is confined within a channel or it is parameterized in terms of the Ekman number K ($\beta = 2K = 2(\tau_b/\rho_r H)/(fU) = 2C_d U/fH$) if it is not (see PB94).

The model was run with a number of different initial conditions to investigate the effects of low latitude, seasonal variability, and topography. The source water properties are listed in Table 2: They were derived from the observations described above. The oceanic properties were obtained from the climatological analysis of the NAVOCEANO hydrographic data. We chose the oceanic profiles from a site that was close to the strait exit but that appeared to be the least affected by recently injected outflow water. The locations of the oceanic profiles are also listed in Table 2. The starting position of each outflow was placed where the straits begin to open up onto the continental shelf. Bottom depth and slope were estimated along the outflow path using the ETOPO2 digital bathymetric database.

6.2. Simulations of the Red Sea Outflow

We use the simulation of the Red Sea outflow in winter as our nominal case, shown by the thick lines in Figure 5. The path of the model outflow from the starting point until it reaches neutral buoyancy is shown in Figure 5a. Use of the Ekman number-dependent broadening parameterization (which assumes completely open topography) caused the outflow to broaden far beyond the actual width of the main channel, and hence the width was assumed to be constant for the first 5 km, then to increase at a rate determined by the width of the main channel ($\beta = 0.1$).

The model outflow descends the upper continental slope along the main channel and reaches neutral buoyancy just 40

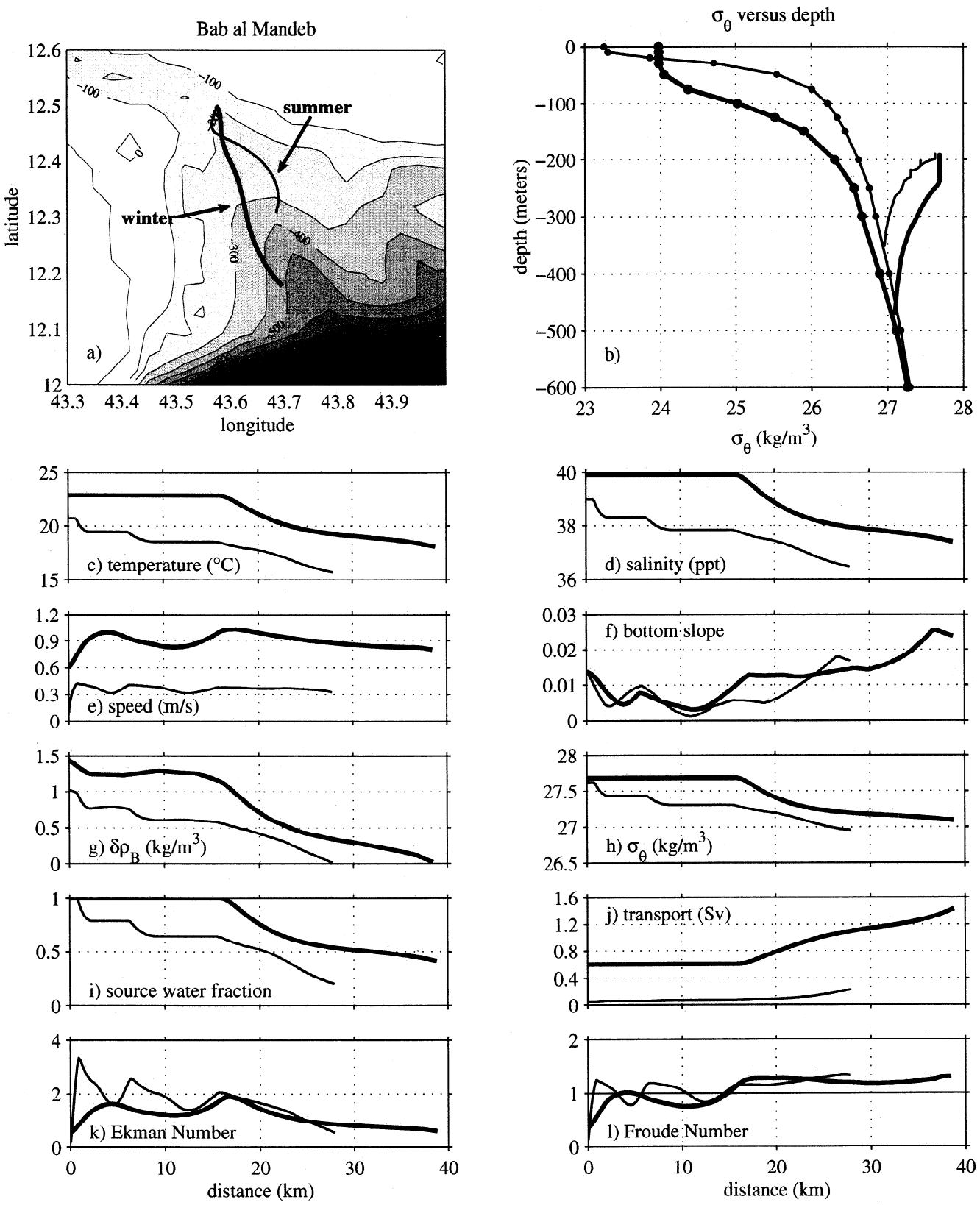

Figure 5. Results from Red Sea outflow model simulations for winter (thick lines), representing the nominal case, and summer (thin lines). Bathymetry in (Figure 5a) is from ETOPO2 digital bathymetric database.

km downstream from the starting location. The outflow evolves in two stages. Over the first 15 km the outflow descends ~50 m without entraining the overlying Gulf of Aden water. Outflow temperature, salinity, density, and transport (Figures 5c, 5d, 5h, and 5j) thus remain unchanged over this distance. Velocity increases from 0.6 m s^{-1} to 1.0 m s^{-1} (Figure 5e) owing to the bottom slope, but the slope is generally below 0.01 (Figure 5f) and the Froude number is below 1 ($Ri > 0.8$, $E = 0$; see equation (4)) (Figure 5l). Starting around 17 km downstream from the starting position, the bottom slope increases above 0.01, U increases to a maximum value just over 1.0 m s^{-1}, the Froude number exceeds 1, and the outflow begins to entrain the overlying water. Up to the point where entrainment begins the outflow has already lost ~30% of its density anomaly because of its descent through the highly stratified upper ocean (Figure 5g). The second (entrainment) stage of the descent continues to 40 km downstream, where the outflow reaches neutral buoyancy at ~475 m depth, and the simulation is terminated. The total elapsed time is only ~0.5 days. Figure 5j shows that the model outflow transport increases by a factor of ~2.5 due to entrainment (same as estimated from observed T-S characteristics, Figure 4), and the final outflow properties are $\theta = 18.1°C$, $S = 37.4$, and $\sigma_\theta = 27.1$. These values are not very different from those obtained from the hydrographic data for the bulk properties of the product water, 17.9°C, 37.5, and 27.2. Note that the outflow becomes neutrally buoyant before reaching the Tadjura Rift, i.e., while still confined within the main channel (Figure 5a).

This model representation of the Red Sea outflow is similar in some ways to that of the Mediterranean outflow described by PB94. Both outflows initially descend the upper continental slope without entraining, then they both begin to entrain cooler and fresher overlying water where the continental slope steepens and the outflow current accelerates. Both outflows more than double their transport owing to entrainment within 40 km of the starting position. Beyond that the dynamics of the two outflows are quite different, due mainly to the lower latitude of the Red Sea outflow. The Ekman number, the ratio of the frictional and Coriolis forces, is $O(1)$ in the Red Sea case ($K = C_d U/fH = (3\times10^{-3})(1 \text{ m s}^{-1})/(3\times10^{-5} \text{ s}^{-1})(100 \text{ m}) = 1$; see also Figure 5k), compared to 0.2-0.4 for the Mediterranean case. Thus the Red Sea model outflow can be characterized as a frictionally damped gravity current modified by rotation rather than a nearly geostrophic gravity current slightly modified by friction. Rotation has some effect in that the model outflow does not plunge down the steepest slope but stays somewhat to the right of the channel axis (facing downstream) (Figure 5a).

To test this characterization of the Red Sea outflow, the model was rerun using latitudes of 37°N and 75°N. This lowered the Ekman number to values similar to the Mediterranean case. In these simulations the outflow path turns to the right and descends the slope less steeply than in the nominal case, as would be expected for a nearly geostrophic density current (see, e.g., PB94). In the 75°N case the model outflow descends the slope so gradually that it reaches the edge of the Tadjura Rift (where bottom slope becomes very steep, exceeding 0.06) before equilibrating. However, interestingly, the product water properties in these two higher-latitude simulations are not significantly different from the nominal case: E.g., at 75°N, where the Ekman number is ~0.2, the equilibrium depth of the product water is only 20 m deeper than for the nominal case. While the low latitude of the Red Sea outflow affects its path somewhat, the latitude does not strongly influence the product water properties in these simulations.

It is interesting to note that the Red Sea model outflow still has a significant speed (~0.8 m s^{-1} (Figure 5e) when it reaches neutral buoyancy). The present model cannot be used to investigate the consequences, but we speculate that the current will undergo geostrophic adjustment with some of the kinetic energy converted to potential energy in the adjustment process. This would result in a banking up against the boundary and a boundary current, perhaps as indicated by some of the observations described above. The RSW properties would presumably continue to evolve downstream because of (primarily lateral) mixing with the surrounding water.

6.3. Sensitivity to Other Model Parameters

Before continuing with an investigation of the effects of seasonal variability and topography on product water properties, the sensitivity of the product water to plausible variations in source water properties, including the outflow's initial direction, transport, and density, was examined. The model results were found to be insensitive to changes in initial outflow direction: ±30° variations produced equilibrium depth differences of < 5 m and no discernible effect on product water temperature, salinity, or source water fraction. Variations in initial outflow transport of ±0.2 Sv around the nominal winter value of 0.6 Sv (indicated by the observations of *Murray and Johns* [1997] produced relatively minor changes in product water properties: ±20 m in equilibrium depth, ±0.5°C in temperature, and ±0.04 (10%) in source water fraction. Higher initial transport results in less entrainment and thus a slightly warmer, saltier and denser product water. As was suggested by PB94, such transport variations may lead to small along-stream variations in RSW product water properties.

The observed seasonal variability in source water density is quite small (0.06 kg m^{-3}, see Table 2 and section 3). To investigate the effect of possible long-term (climatic) changes in source water characteristics, source water salinity variations of ±0.5 were imposed (±0.6 kg m^{-3} in density). This led to variations of ±50 m in equilibrium depth, ±1°C in temperature, and ±0.1 (25%) in source water fraction. When the initial salinity (and density) is higher, the outflow entrains more, and the product water is cooler and fresher. However, as was pointed out by PB94 for the Mediterranean case, most of the initial density variation is lost in the entrainment process (~77% in the Red Sea simulations). On the basis of these results we conclude that realistic (observed) variations in initial direction, transport, and source water density have only a minor impact on product water properties in the present model.

Sensitivity to the choice of critical Richardson number was also tested: for variations from 0.6-1.0 (nominal value was 0.8), equilibrium depth of the product water varied from 530-435 m, product water temperature varied from 18.1°C to 18.2°C, and source water fraction varied from 0.44 to 0.40. The main effect of altering the critical Richardson number is to change where the outflow begins entraining. For example, increasing the critical Richardson number causes the model

outflow to begin entraining earlier and thus higher in the water column. In the Red Sea simulation, this results in the entrainment of warmer, fresher water and thus the production of a slightly warmer, fresher, less dense product water. Again, however, the effect on product water properties is relatively minor for variations of the critical Richardson number over the range noted.

6.4. Seasonality

In previous studies of the Red Sea outflow it has been suggested that the characteristics of the product water may vary as a function of season. For example, *Maillard and Soliman* [1986] suggested that RSW equilibrates at shallower depths in winter and perhaps as deep as 1000-1200 m in summer and is cooler by several degrees in summer. The thin lines in Figure 5 show the results for a model run with summer initial conditions (see Table 2). The outflow initially accelerates from 0.1 m s^{-1} to 0.4 m s^{-1} (Figure 5e) owing to the bottom slope, and H, which started out low (50 m) because of the low transport, decreases even more (< 25 m) (not shown). The Ekman number is around 2 (Figure 5k), indicating that the summer outflow is even more frictional than the winter outflow. As a result, the summer outflow follows a path nearly down the middle of the channel (Figure 5a). Also, the Froude number exceeds 1 almost immediately after starting, and the outflow begins entraining sooner than in winter (Figure 5l). Entrainment occurs intermittently as the flow accelerates and decelerates in response to changes in slope (Figures 5e and 5f). At 20 km downstream the slope increases significantly, and the entrainment occurs continuously onward until the outflow reaches neutral buoyancy at ~350 m, some 30 km downstream from the starting point. The summer outflow entrains less volume than winter (0.2 Sv compared to 0.8 Sv), but the dilution factor (relative entrainment) is much greater (4.8 versus 2.5) because of the much lower initial transport (0.05 Sv versus 0.6 Sv; see section 6.3).

The summer model product waters are cooler and fresher than the product water in winter (15.6°C and 36.5 in summer compared to 18.1°C and 37.4 in winter), due largely to the greater dilution in summer. This seasonal difference in product water temperature is roughly as observed in the AXBT data, although the model summer product water temperature is ~1.5°C cooler than the mean of the summer temperature maxima observed from AXBT observations (see section 3). On the other hand, a recent hydrographic section along the axis of the Gulf of Aden in August-September 1995 shows evidence of product waters with a T-S of 15°-16°C and 36.5-36.75 centered at ~450 m, rather similar to the present model results [*Mecking and Warner*, 1999]. Because the summer outflow entrains much more oceanic water, the product water properties will be quite sensitive to the oceanic properties. The summer model outflow equilibrates ~125 m shallower than the winter outflow (contrary to the suggestion of *Maillard and Soliman* [1986]) because of its slightly lower density (26.9 compared to 27.1) and the different oceanic stratification (Figure 5b). In order for the model to produce product water at depths of 1000-1200 m the oceanic density profile would have to be nearly uniform with depth, which it clearly is not.

6.5. Topography

Fedorov and Meshchanov [1988] showed schematically that RSW exiting the strait through the northern channel maintains its source water characteristics for a longer distance downstream than does the RSW following other pathways. This northern channel is very narrow (~5 km) and extends for ~80 km, over which the bottom depth increases from ~200 m to 650 m [*Siedler*, 1968]. Since this feature is not resolved in the ETOPO2 digital database, we have replaced the realistic bathymetry by a plane with slope 0.005 and kept the outflow width fixed at 5 km until it reaches 650 m depth, at which point the slope increases to 0.07, and the width is allowed to increase according to the Ekman number-dependent parameterization of broadening. This is meant to crudely simulate the northern channel and its opening onto the steep slope associated with the Tadjura Rift. We otherwise used the same parameters as for the nominal winter simulation except that the initial transport is half of the total, assuming that only a part of the outflow follows this channel (see Table 2).

The results of this northern channel simulation are shown in Figure 6. Since the model outflow is not confined by sloping channel walls, its path in geographic coordinates is meaningless and is not shown. To ensure that this does not affect the main results, a run with f set to 0 (causing the outflow to go straight down the slope) was performed. This run gave similar results (see below). The model outflow initially accelerates to 1 m s^{-1} because of the bottom slope (Figure 6d), the Froude number exceeds 1 starting at ~10 km downstream (Figure 6k), and weak entrainment begins. Entrainment stops at ~75 km, mostly because the outflow speed has decreased to ~0.7 m s^{-1} (Figure 6d). At this point, outflow transport has increased by ~20% (Figure 6i), and temperature and salinity have decreased only moderately to 21.5°C and 39.2, respectively, (Figures 6b and 6c). The outflow then continues to descend (and lose buoyancy, Figure 6f) without entraining. When it reaches the steeper slope at the end of the channel, it accelerates and broadens and quickly entrains enough overlying water to reach neutral buoyancy at a depth of ~800 m. This is 325 m deeper than in the nominal winter case. The product waters are significantly warmer, saltier, and denser than in the nominal run (20.5°C, 38.8, and 27.5), and the transport has increased by only ~35%. (In the $f = 0$ case the outflow entrains at a slow rate all along the channel and reaches equilibrium at ~650 m. While not quite as deep as the 12°N run, the depth, temperature, salinity, and density are still significantly different from those in the main channel case.)

Two important differences are apparent between this and the nominal case. First, the combination of weak bottom slope and the narrowness of the northern channel allow the outflow to descend much deeper (to ~650 m) without entraining much oceanic water, thus preserving the source water characteristics to greater depths. This feature is also seen clearly in the observations; *Siedler's* [1968] Figures 21-23 show only small changes in the temperature, salinity, and density of the outflow in sections along the axis of the northern channel made in November-December 1964. At the exit of the channel (650 m isobath) the observed outflow was still at the bottom (i.e., not floated off), and its temperature, salinity, and density were 20°-21°C, 39.5-40, and 27.5-28. Second, these relatively

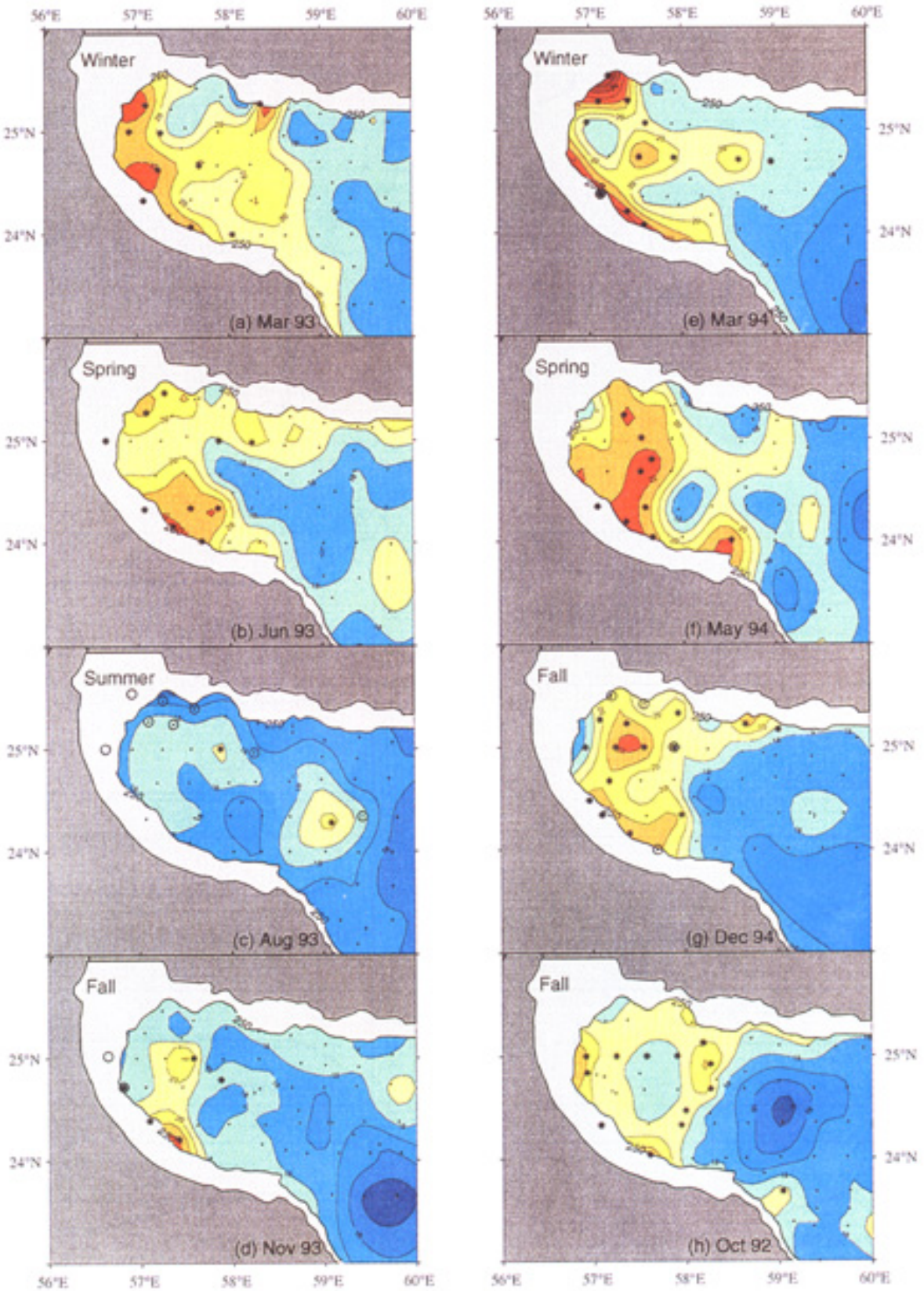

Plate 10. Synoptic temperature distributions at 250 m in the Gulf of Oman during eight AXBT surveys. Small dots indicate station locations, and symbols show the locations of intermediate temperature maxima deeper than 175 m (asterisks) and shallower than 175 m (circles).

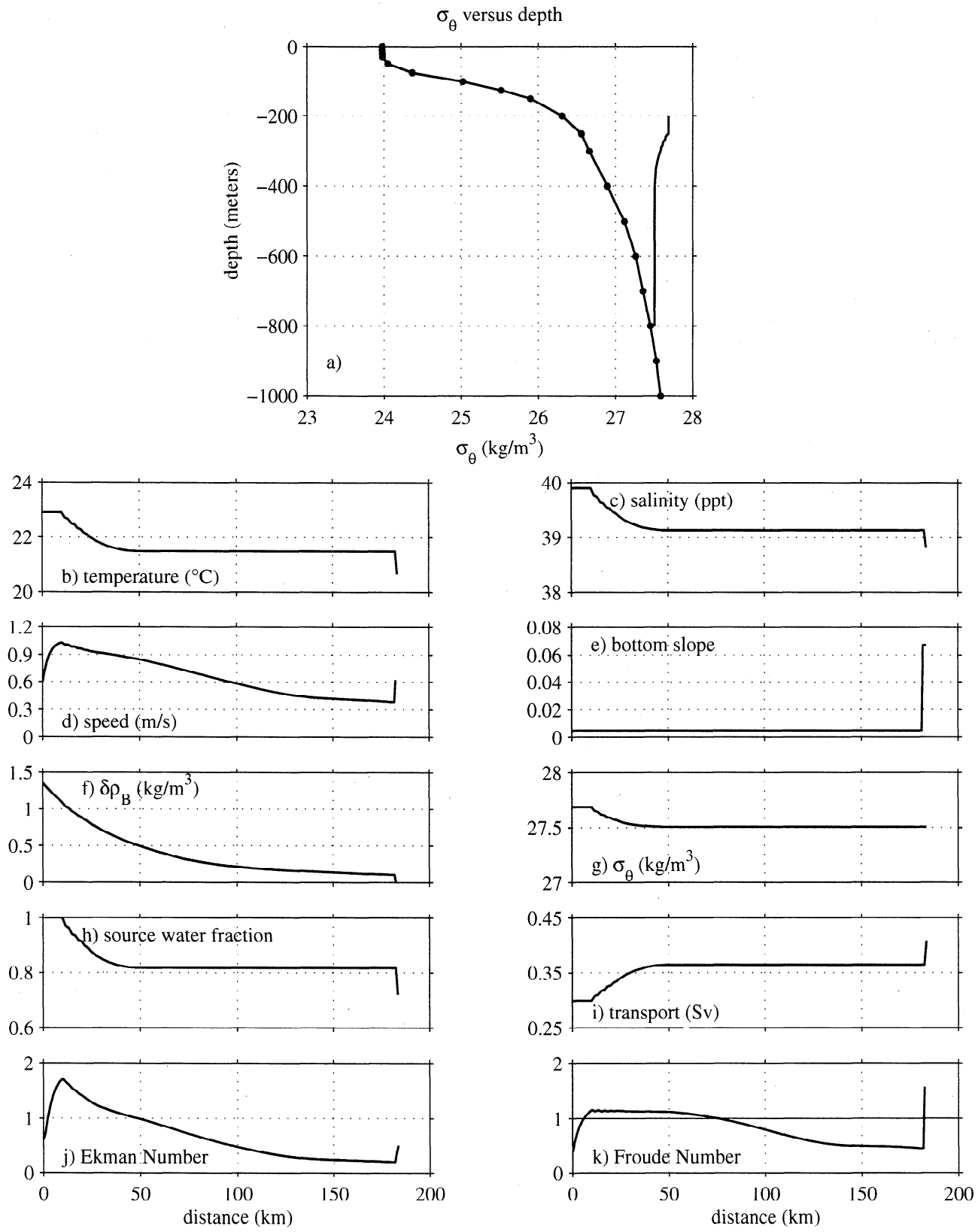

Figure 7. Same as for Figure 5 but for the Persian Gulf outflow model simulations.

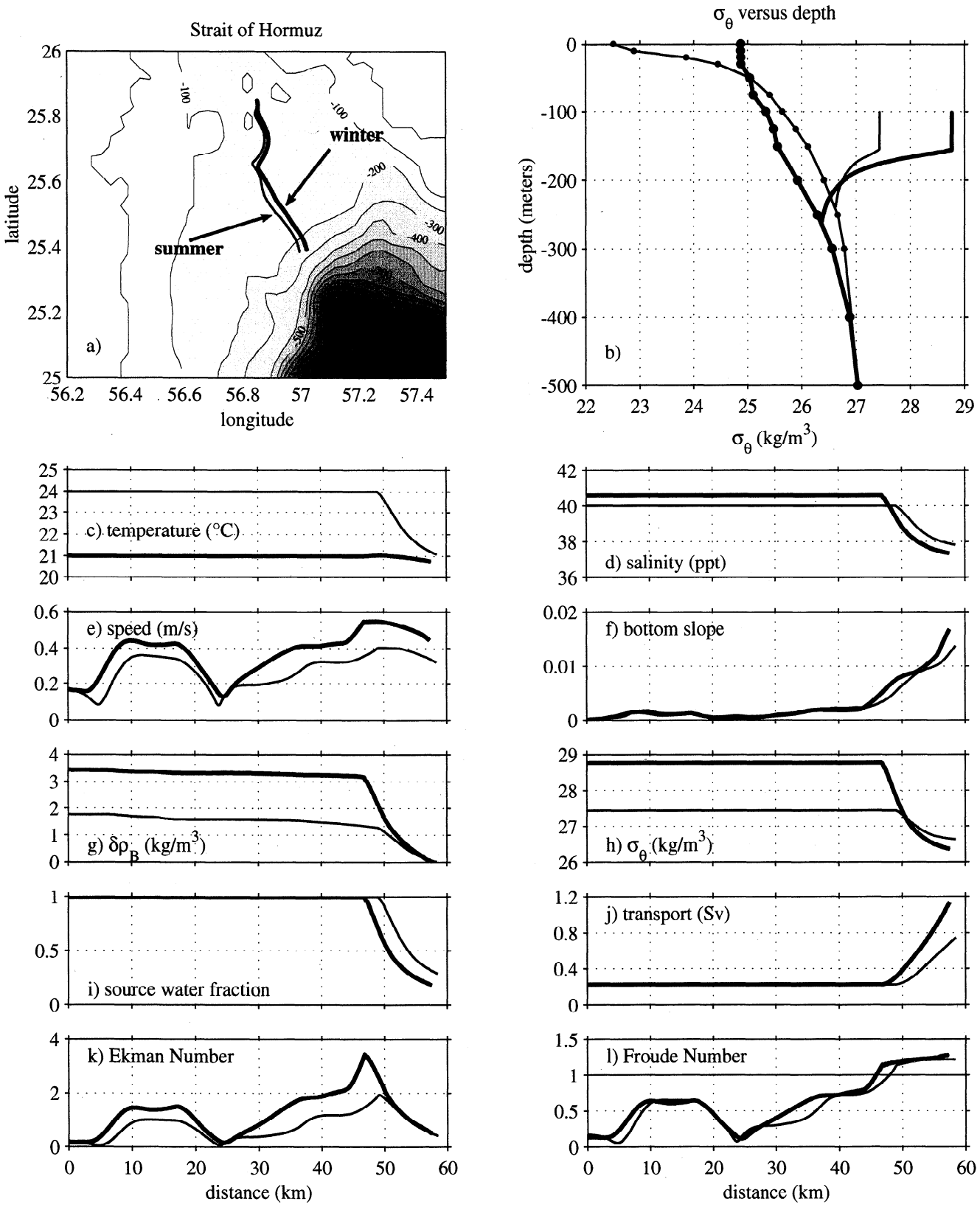

Figure 6. Same as for Figure 5 but showing results of the Red Sea outflow simulation in the northern channel.

undiluted source waters are injected into the oceanic environment below the highly stratified upper thermocline. This northern channel outflow thus entrains comparatively dense oceanic water and consequently equilibrates at a deeper depth than does the main channel outflow.

6.6. Simulations of the Persian Gulf Outflow

The initial conditions for the Persian Gulf outflow simulations are listed in Table 2. Compared to the Red Sea outflow, this outflow is more dense, has a lower initial transport, and is wider. Note also that the summer source water is ~3°C warmer, 0.2 fresher, and thus less dense by ~1.3 kg m^{-3} compared to the winter source water (Table 2). As was found in the Red Sea case, the model Persian Gulf outflow widened at a rate that was unrealistically large when the Ekman number-dependent parameterization for outflow width was used, so outflow width was modeled as a widening channel constrained first by the 100 m isobath and then the 200 m isobath ($\beta = 0.6$).

The Strait of Hormuz opens out onto the continental shelf, where bottom slopes are relatively weak (< 0.005) (Figures 7a and 7f). The Froude number is below 1 over the shelf in both summer and winter (Figure 7l), so there is no entrainment as the outflow crosses the shelf. As the outflow widens and speeds up in response to slight changes in bottom slope on the shelf (Figure 7e), H decreases to 10-20 m (not shown), and the Ekman number exceeds 1 (Figure 7k). This indicates that even at this higher latitude (26°N), the model outflow is strongly influenced by friction, primarily because it is very thin.

About 45 km from the starting position the model outflow reaches the edge of the continental shelf (150 m isobath). Here the slope increases sharply (reaching 0.014, Figure 7f), and the outflow speed increases to a maximum of 0.55 m s^{-1} (winter) and 0.40 m s^{-1} (summer). The winter outflow accelerates more owing to its higher initial density anomaly (3.4 kg m^{-3} versus 1.8 kg m^{-3} in summer, Figure 7g). In both seasons, the Froude number goes above 1 at this point (Figure 7l), and entrainment begins. The winter outflow temperature first increases slightly since the overlying Gulf of Aden water is warmer than the outflow in winter. The final dilution factors are 4.9 in winter, and 3.3 in summer, which bracket the value estimated from the composite T-S diagram (Figure 4). The winter and summer product waters have similar temperatures, 20.8°C and 21.0°C, respectively (Figure 7c): The summer outflow starts out warmer, but since the dilution factors are so high, the product water properties are dominated by the oceanic temperatures in both seasons, which are not that different over the depth range of entrainment, ~150-250 m. The summer product water salinity is ~0.5 higher than winter and thus somewhat more dense (26.6 versus 26.3), but because of the different oceanic stratification in summer and winter the product waters end up at about the same depth in both seasons, ~250 m (Figure 7b). As was the case for the Red Sea simulations, the model Persian Gulf outflow has significant momentum when it reaches the depth at which it is neutrally buoyant (Figure 7e). The greater density anomaly in winter may explain why better defined boundary currents of Persian Gulf product water are observed in winter (see Plate 10).

7. Summary and Conclusions

We have used historical hydrographic data and the one-dimensional, steady outflow model of *Price and Baringer* [1994] to investigate the initial transformation, dynamics, and spreading pathways of Red Sea and Persian Gulf outflow waters where they enter the Indian Ocean. These two outflows are different from the major Atlantic outflows in several ways. They flow over very shallow sills (depth < 200 m) into a well-stratified upper ocean environment and entrain much less dense overlying water as they descend the continental slope until they reach equilibrium in the Indian Ocean (nominally at ~600 m for the Red Sea outflow and ~250 m for the Persian Gulf outflow). Their annual mean transport is small (< 0.4 Sv in both cases), and in the Red Sea case, there is a strong seasonal cycle in outflow transport. They are also located at relatively low latitudes, 12°N and 26°N.

The observations were first used, along with results from previous studies, to document the seasonal variability in outflow source water (before significant entrainment occurs), product water (after entrainment stops), and oceanic water properties. Summarizing our results from this analysis, we found that Red Sea source water is cooler (by ~2°C) and lower in salinity (by ~1) in summer owing to mixing with Gulf of Aden water in Bab-el-Mandeb Strait, although these effects compensate, such that source water density is about the same in summer and winter. Multiple layers of recently injected equilibrated Red Sea product water often coexist and can be traced for up to several hundred kilometers in narrow veins along the western and southern slopes of the Gulf of Aden. Product water temperatures are generally lower by ~2°C in summer.

The Persian Gulf source water is ~3°C warmer in summer compared to winter, which is only partially compensated for by salinity, resulting in a less dense source water in summer. This is probably related to the seasonal heating cycle over the shallow Persian Gulf. In the summer and fall observations in the Gulf of Oman we found evidence of product water that is warmer (by several degrees) and shallower (by 50-100 m) than the classical product water, which may result from the warmer, less dense source waters observed at that time of year. The equilibrated Persian Gulf outflow water, like the Red Sea outflow water, also appears to be advected away from its source by a narrow boundary current flowing along the upper continental slope of the western and southern Gulf of Oman. This feature is quite variable seasonally: most continuous in winter, patchy in spring and fall, and not apparent in summer.

On the basis of the observed T-S characteristics of the outflow source and product waters and the oceanic water we estimate that the Red Sea and Persian Gulf outflows are diluted by factors of ~2.5 and 4, respectively, as they descend from sill depth to their depth of neutral buoyancy. The Red Sea dilution factor is similar to that for the Mediterranean outflow. The high dilution factor for the Persian Gulf outflow, which is higher than for any of the Atlantic outflows, results from the combined effects of the large initial density difference between the outflow and oceanic water and low outflow transport.

Using the observed geophysical characteristics of these two outflows, we found that the combination of low latitude and

low outflow transport (and associated low outflow thickness) results in Ekman numbers for both outflows that are $O(1)$. This indicates that they can be characterized as frictional density currents modified by rotation, rather than geostrophic density currents modified by friction. As a result, they tend to flow down the continental slope at a steep angle, rapidly entraining the overlying water and reaching neutral buoyancy just a short distance from the shelfbreak (< 30 km). This is in contrast to the Atlantic outflows, which turn to more or less follow the isobaths of the continental slope as nearly geostrophic density currents before they reach neutral buoyancy.

The numerical plume model was run with various initial conditions to investigate the effects of low latitude, seasonal variations in source and oceanic properties, and topography on the product water properties of the Red Sea and Persian Gulf outflows. Considering both the seasonal and topographic effects on the Red Sea outflow, it seems that topography is more important in generating Red Sea product waters with significantly different densities. The main channel directing Red Sea water into the open ocean is the likely source region for the product waters < 500 m, and the very narrow, gently sloping northern channel produces deeper layers, 600-800 m.

What is not clear from this analysis is how the highly saline Red Sea outflow waters observed below 1000 m are produced. As pointed out by PB94, with the physical processes represented in this model it is virtually impossible to end up with product waters at the bottom of the receiving basin if the outflow is injected into a stratified environment. The product water below 1000 m is confined to the Tadjura Rift and nearly closed off from the Gulf of Aden. One might speculate that the deep product water has been in the rift for some time and was formed when the stratification of the gulf was weaker. This is not supported by recent chlorofluorocarbon (CFC) observations in the Gulf of Aden, which indicate that the deep water in the rift has been recently ventilated [*Mecking and Warner*, 1999]. Alternatively, there may be important physical processes at work that are not represented in the model. For example, *Fedorov and Meshchanov* [1988] suggested that double-diffusive convective mixing at the top interface of the outflow layer before it floats off the bottom results in a significant loss of heat with no change in salinity and thus an increase in density. There is evidence of strong step-like features in many of the temperature and salinity profiles used here. The high CFC concentrations of the deep saline layer argue against the possibility of a hydrothermal source, although the nearby Red Sea is known for its deep, salty brines [*Degens and Ross*, 1969]. More observations are needed to determine the source of this deep water mass.

The numerical model produces Persian Gulf product waters in summer and winter with somewhat different *T-S* properties, but it equilibrates at the classical, 250-m depth of PGW in both seasons. This is in spite of the considerable difference in source water temperature and density. The shallow, warm product waters observed in some of the summer observations were not produced by the model. As was pointed out by PB94, the model outflow product water characteristics are in many ways more sensitive to the oceanic rather than source water properties. This is especially true for the Persian Gulf outflow, which entrains 4-5 times its initial transport.

The analyses presented here provide a first look at the transformation of water properties, dynamics, and initial spreading pathways of the Red Sea and Persian Gulf outflows. A number of intriguing questions remain to be addressed.

1. How do these outflows evolve in the critical first 30 km downstream from the shelfbreak? The observations analyzed here were not of sufficient resolution to examine the structure of the outflow plumes as has been accomplished for other marginal sea outflows.

2. What is the source of the warm, saline water found in the bottom of Tadjura Rift? The physical processes represented in our crude outflow model cannot transport product water below ~800 m. Perhaps the double-diffusive convective layering mechanism suggested by *Fedorov and Meshchanov* [1988] is important. Also, the model showed how two different densities of Red Sea product water could originate from the two channels, but there are sometimes more than two layers observed. Where do they originate?

3. How do tides and other higher-frequency current fluctuations affect the product water properties? Because the Red Sea outflow equilibrates in < 1 day, baroclinic tides may contribute to some of the observed variability in product water characteristics. New observations are required to address this issue.

4. How do the descending outflow plumes evolve into a wall-bounded jet after reaching gravitational equilibrium? The model runs suggest that they may still have significant momentum at this point. Is there a geostrophic adjustment process that turns the outflow current to the right where it can "lean" against a boundary?

5. Why does the Persian Gulf outflow transport appear to be relatively steady throughout the year even though the density difference between the outflow and the oceanic water is 60% lower in summer? Could differential surface heating between the Persian Gulf and the Gulf of Oman counter this trend and lead to a more or less constant pressure difference between the two areas?

In order to address these questions and more fully understand the dynamics of these two unique marginal sea outflows, high-resolution, synoptic observations of temperature, salinity, and velocity are needed.

Acknowledgments. We gratefully acknowledge Jeff Kerling of the U.S. Naval Oceanographic Office, without whose enthusiasm, interest, and expertise this study would not have been possible. Carol Alessi modified the HydroBase utility package for use with the NAVOCEANO data set and doggedly applied the quality control procedure in this challenging area. We are extremely grateful to Bill Johns of the University of Miami for sharing unpublished results from his moored instruments in the Strait of Hormuz. Insightful comments from several anonymous reviewers are also gratefully acknowledged. This work was supported by grant N00014-95-1-0284 to the Woods Hole Oceanographic Institution from the U. S. Office of Naval Research. This is contribution 9548 from the Woods Hole Oceanographic Institution.

References

Ahmad, E., and S. A. R. Sultan, Annual mean surface heat fluxes in the Arabian Gulf and the net heat transport through the Strait of Hormuz, *Atmos. Ocean, 29(1), 54-61*, 1991.

Alessi, C. A., H. D. Hunt, and A. S. Bower, Historical data from the US Naval Oceanographic Office: Persian Gulf, southern Red Sea

and Arabian Sea 1923-1996, *Tech. Rep. WHOI-99-02*, Woods Hole Oceanogr. Inst., Woods Hole, Mass., 1999.

Ambar, I., and M. R. Howe, Observations of the Mediterranean outflow, I, Mixing in the Mediterranean outflow, *Deep Sea Res., Part A, 26*, 535-554, 1979a.

Ambar, I., and M. R. Howe, Observations of the Mediterranean outflow, II, The deep circulation in the vicinity of the Gulf of Cadiz, *Deep Sea Res., Part A, 26*, 555-568, 1979b.

Beal, L. M., A. Field, and A. L. Gordon, Spreading of Red Sea overflow waters in the Indian Ocean, *J. Geophys. Res.*, in press, 1999.

Bower, A. S., L. Armi, and I. Ambar, Lagrangian observations of meddy formation during a Mediterranean undercurrent seeding experiment, *J. Phys. Oceanogr., 27*, 2545-2575, 1997.

Boyd, J. D., Improved depth and temperature conversion equations for Sippican AXBTs, *NORDA Rep. 156*, 6 pp., Nav. Oceanogr. and Atmos. Res. Lab., Stennis Space Center, Miss., 1986.

Brewer, P. G., A. P. Fleer, S. Kadar, D. K. Shafer, and C. L. Smith, Chemical oceanographic data from the Persian Gulf and Gulf of Oman, *Tech. Rep. WHOI-78-37*, 105 pp., Woods Hole Oceanogr. Inst., Woods Hole, Mass., 1978.

Chao, S.-Y., T. W. Kao, and K. R. Al-Harji, A numerical investigation of circulation in the Arabian Gulf, *J. Geophys. Res., 97*, 11,219-11,236, 1992.

Curry, R. G., HydroBase–A database of hydrographic stations and tools for climatological analysis, *Tech. Rep. WHOI-96-01*, 44 pp., Woods Hole Oceanogr. Inst., Woods Hole, Mass., 1996.

Degens, E. T., and D. A. Ross (Ed.), *Hot Brines and Recent Heavy Metal Deposits in the Red Sea*, Springer-Verlag, New York, 1969.

Fedorov, K. N., and S. L. Meshchanov, Structure and propagation of Red Sea Waters in the Gulf of Aden, *Oceanology, 28*, 279-284, 1988.

Horton, C., M. Clifford, J. Schmitz, and B. Hester, SWAFS: Shallow Water Analysis and Forecast System Overview and Status Report, NAVOCEANO Report, 54 pp., U.S. Nav. Oceanogr. Off., 1994.

John, V. C., S. L. Coles, and A. I. Abozed, Seasonal cycles of temperature, salinity and water masses of the Western Arabian Gulf, *Oceanol. Acta, 13*, 273-281, 1990.

Maillard, C., and G. Soliman, Hydrography of the Red Sea and exchanges with the Indian Ocean in summer, *Oceanol. Acta, 9*, 249-269, 1986.

Mecking, S., and M. J. Warner, Ventilation of Red Sea Water with respect to chlorofluorocarbons, *J. Geophys. Res.,104*, 11,087-11,097, 1999.

Morcos, S. A., Physical and chemical oceanography of the Red Sea, *Oceanogr. Mar. Biol. Ann. Rev., 8*, 73-202, 1970.

Murray, S. P., and W. Johns, Direct observations of seasonal exchange through the Bab el Mandab Strait, *Geophys. Res. Lett., 24*, 2557-2560, 1997.

Osman, M. M., Water exchange between the Red Sea and Gulf of Aden, *Simp. Int. Afloramiento O Africa., Inst. Invest. Pesq. Barcelona, 1*, 205-212, 1985.

Patzert, W. C., Seasonal reversal in Red Sea circulation, in *L'Oceanographie Physic de la Mer Rouge*, pp. 55-89, United Nations Educ., Sci., and Cult. Org., Paris, 1972a.

Patzert, W. C., Volume and heat transports between the Red Sea and Gulf of Aden, and notes on the Red Sea heat budget, in *L'Oceanographie Physic de la Mer Rouge*, pp. 191-201, United Nations Educ., Sci., and Cult. Org., Paris, 1972b.

Premchand, K., J. S. Sastry, and C. S. Murty, Water mass structure in the western Indian Ocean, part 2, The spreading and transformation of the Persian Gulf Water, *Mausam*, 37, 179-186, 1986.

Price, J. F., and M. O. Baringer, Outflows and deep water production by marginal seas, *Prog. Oceanogr., 33*, 161-200, 1994.

Privett, D. W., Monthly charts of evaporation from the North Indian Ocean, including the Red Sea and the Persian Gulf, *Q. J. R. Meteorol. Soc., 85*, 424-428, 1959.

Quadfasel, D., and N. Verch, Seasonal variability of temperature in the Red Sea: XBT-sections from MCS "UBENA" in 1985 and 1986, *Tech. Rep. 1-87*, 25 pp., Inst. fur Meereskunde, Univ. Hamburg, Hamburg, Germany, 1987.

Rochford, D. J., Salinity maxima in the upper 1000 metres of the north Indian Ocean, *Aust. J. Mar Freshwater Res., 15*, 1-24, 1964.

Shapiro, G. I., and S. L. Meshchanov, Distribution and spreading of Red Sea Water and salt lens formation in the northwest Indian Ocean, *Deep Sea Res., Part A, 38*, 21-34, 1991.

Siedler, G., Schichtungs- und Bewegungsverhaltnisse am Sudausgang des Roten Meeres, *Meteor Forschungsergeb., Reihe A, 4*, 1-76, 1968.

Siedler, G., General circulation of water masses in the Red Sea, in *Hot Brines and Recent Heavy Metal Deposits in the Red Sea*, edited by E. T. Degens and D. A. Ross, pp. 131-137, Springer-Verlag, New York, 1969.

Varma, K. K., V. K. Das, and A. D. Gouveia, Thermohaline structure and watermasses in the Northern Arabian Sea during February-April, *Indian J. Mar. Sci., 9*, 148-155, 1980.

Wyrtki, K., Oceanographic Atlas of the International Indian Ocean Expedition, Nat. Sci. Found., Washington, D. C., 531 pp., 1971.

A. Bower, H. D. Hunt, and J. F. Price, Department of Physical Oceanography, Woods Hole Oceanographic Institution, Woods Hole, MA 02543. (abower@whoi.edu)

(Received July 16, 1997; revised October 12, 1999; accepted October 13, 1999.)